THE NATURE OF HYPERELECTRONIC POLARIZATION

By

JOHN RIORDON WYHOF
)\

Bachelor of Arts
Middlebury College
Middlebury, Vermont
1965

Master of Science
Oklahoma State University
Stillwater, Oklahoma
1967

Submitted to the Faculty of the Graduate College
of the Oklahoma State University
in partial fulfillment of the requirements
for the degree of
DOCTOR OF PHILOSOPHY
May, 1970

Thesis
1970
Corral
W979n
cop. 2

THE NATURE OF HYPERELECTRONIC POLARIZATION

Thesis Approved:

Herbert A. Pohl
_____
Thesis Adviser

_____

James Lange
_____

Leonel M. Raff
_____

N. Durham
_____
Dean of the Graduate College

762871

ACKNOWLEDGEMENTS

Research Institute, for granting him a Research Fellowship.

Finally, he expresses his appreciation to his wife, Nancy Lou, for her patience and encouragement, and for her aid in the preparation of this manuscript.

TABLE OF CONTENTS

LIST OF TABLES

LIST OF FIGURES

CHAPTER I

INTRODUCTION

Research on organic semiconductors has in recent years yielded
considerable data on the electrical properties of polymers in the solid
state. One of the most intriguing observations was the phenomenon of
hyperelectronic polarization in conducting polymers (1). This term has
been given to an extraordinarily high polarization which cannot be
explained by the conventional mechanisms of electronic, atomic, dipole
or interfacial polarization (2).

Hyperelectronic polarization is due to the induced moments of mo-
bile charges on long molecules. The mobile charges are produced by ex-
citation of charge pairs called Mott excitons lying on different mole-
cules. This charge is then confined to the molecule and moves essen-
tially without resistance along the molecule. If there is no external
electric field, the resulting total polarization will be zero, although
there may be domains which have a net polarization. When a small exter-
nal field is applied, the charges are displaced and a net polarization
is observed which is much greater than can be accounted for by conven-
tional mechanisms. Permittivities as high as 300,000 have been observed
in these polymers.

Electronic polarization, due to the small shift of the positive and
negative charge in the atoms, is proportional to the applied field. The
shift of the electron cloud center is of the order of 10^{-9} angstroms for

fields of 10^4 volts/cm. Atomic polarization, or displacement of charged atoms with respect to each other, produces an induced dipole polarization on an atomic scale. A ground state asymmetric charge distribution in molecules gives rise to permanent dipoles resulting in dipolar polarization. These types of polarization are locally bound to the atoms or molecules and result in the normal permittivity, 2-10, observed for most organic solids.

Interfacial or Maxwell-Wagner polarization is due to trapped carriers at interfaces within the material. The interfaces may consist of discontinuities due to grain boundaries, or differences in composition as in solid mixtures. If the charge becomes stored at such an interface, large increases in polarization are observed. This type of polarization is somewhat analogous to hyperelectronic polarization except that in the latter the charge is trapped or stored in long molecules instead of macroscopic interfaces.

The observation of hyperelectronic polarization rather than Maxwell-Wagner polarization has been clearly shown by Hartman (3) for conjugated polymers of the type investigated here. The polymers examined were composed of highly purified materials. The samples were measured under conditions of high pressure up to 20,000 atmospheres. This pressure is ten times the compressive or tensile strength of known organic polymers. It was observed that the dielectric constant increased very smoothly with pressure and temperature, indicating only molecular scale polarization. It had been argued that the conducting polymer is surrounded by a thin layer of poorly conducting polymer. The samples were exposed to a 3° shear ten times while under a pressure of 2.5 kilobars. The measured permittivity was unchanged by this shearing, thus showing a truly

homogenous material in a single phase. The surface layer effect between the polymer sample and electrode might also have been a cause for the high permittivities. In the investigation by Hartman the sample thickness and electrode material were varied. No detectable differences in measured permittivities were found.

The study concluded that hyperelectronic polarization was the principal contribution to the high polarizabilities of long polymeric, ekaconjugated, macromolecular solids.

Review of the Literature

This investigation concerns the conducting and dielectric properties of a certain class of molecular solids; namely, the conjugated polymers. The basic theoretical and experimental techniques were developed in earlier studies with organic molecules. One of the earliest papers related to the current studies appeared in 1941 when Szent-Gyorgyi (4,5) suggested the relationship of semiconduction to the field of biochemistry. In 1948 Eley (6) proposed that electrons lie in energy bands common to the whole crystal, arising perhaps from intermolecular overlap of the π-orbitals.

One of the early groups working in the field was headed by Inokuchi. In the early nineteen fifties he published several papers containing conductivity and activation energy data for some eighteen molcular solids (7-9). He assumed that the samples were intrinsic semiconductors, and the conduction was attributed to the π-electrons. In 1954 a good conducting ($1-10^{-3}$ ohm^{-1} cm^{-1}) organic material, perylene-bromine complex, was studied, but it was found to be unstable (10). In the latter part of that decade Inokuchi published conductivity data, including the

effects of pressure (11) on other molecular complexes (12,13). In the early nineteen sixties Inokuchi and coworkers (Shirotani, Minonura and Maruyana) concentrated their efforts on the effects of high pressure on the conductivity, including theoretical treatment (14) of the phenomena (15-17). At the same time Matsunaga (18,19) and Kuwatta (20,21) investigated the magnetic properties of molecular complexes. Particular interest was taken in the electron spin resonance and its relation to temperature and conductivity.

In England Eley's group, publishing in the early nineteen fifties, investigated several organic semiconductors (22,23). He discussed the mobile π-electrons in the conjugated bonds and suggested a theory for the observed energy gap. Continuing with similar investigations, Eley and Spivey reported on semiconduction in proteins and polypeptides (24), porphyrins and copper and cobalt complexes (25), and DNA and RNA in the dry state (26).

Many investigations of covalent, charge-transfer complexes, coordination and hydrogen bonded polymers were made during the past twenty years. These studies concern the relationship of the chemical or molecular structure to the conductivity and electron spin resonance results. An excellent review from the standpoint of chemical structure, including 298 references, has been given by Kanda and Pohl (27).

One of the early uses of pressure on semiconducting organic compounds was reported by Inokuchi in 1955. In studying isoviolanthrone it was noted that the resistivity decreased with applied pressure (28). Further investigations using extreme pressure were reported in the early nineteen sixties by Drickamer's group (29-37). A high pressure apparatus was developed for pressures above 100 kilobars (29). The optical

spectra, conduction and phase transitions were investigated using charge-transfer complexes. Inokuchi continued high pressure investigations (38-40) and attributed the decrease in resistance to an increase in charge carriers. The conductivity increased with pressure for copper-phthalocyanine up to 50 kilobars (41). Further investigations were made on porphyrins (42), charge-transfer complexes (43-44), and copper-phthalocyanine at high pressures (45). A mechanism for the change in activation energy due to the change in pressure was also proposed (46).

Electron spin resonance (ESR) studies have been most useful in understanding the mechanisms of charge carriers in organic semiconductors. Kommandeur has reported on ESR investigations of perylene and pyrene and concluded that the unpaired spins are the charge carriers (47-49). Other electron spin resonance studies included polymers with conjugated bonds and heteroatoms in conjugated chains (50), biradical molecular compounds (51), organic free radicals (52), and organic dyes (53). The ESR spectra was also related to the conductivity for polymers (20,21) and charge-transfer complexes (18, 54-58).

The literature relevant to the study of dielectric properties presented here includes the investigations of measurement techniques and analysis of results. Cole and Cole (59) developed the basic equations for a single relaxation time mechanism. The Cole plots have been expanded to obtain an average dielectric relaxation time (60). A method for determining the loss factor for dielectric measurements (61) and methods for determining the dielectric behavior at low frequencies (62, 63) have been reported. Many investigations have been made on dielectric aspects of molecular solids (64-67) and on interfacial polarization (68-71).

One of the early investigations of the dielectric properties of polymers was reported in 1942 by Baker and Yager (72,73). In 1959 a Russian group investigated the effect of high pressures on the dielectric losses of polymers (74). McCall and Anderson measured the dielectric properties of linear polyamides and proposed that the proton conduction through amorphous regions gives rise to a Maxwell-Wagner loss (75). The dielectric properties of DNA have been discussed by Pollak (76) and Brot (77).

For completeness the theoretical models developed for molecular compounds should be mentioned. Models leading to the present mechanisms used in this study include tight binding approximations (78-82), exciton interactions (83-86), excited states (86,87), molecular orbitals (88-93), tunneling (94), and suggested models for conjugated bond systems (95-100). Hopping (100,101) and trapping models (102) have been developed and applied to polymers.

In 1959 Berlin's group in the USSR reported on the synthesis and ESR measurements of polymers with conjugated bonds (103-106). In 1961 Berlin reported on the electrical properties of newly synthesized conducting polymers (107-109). Semenov discussed low temperature polymerization of polymers with conjugated bonds (110). Paushkin (111) synthesized polymeric semiconductors with conductivities of $10^{-3} - 10^{-6}$ mho/cm and $10^{18} - 10^{19}$ spins/g. Recently Slonimski (112) suggested a method of estimating intermolecular interaction energy in polymers by mechanical stress.

In 1959 McNeill and Weiss synthesized a xanthene polymer with resistivity of 7×10^3 ohm-cm (113). Several other polymers were synthesized and measured by this Australian group (114-116). Attempts were

also made to relate the polymerization time to the observed electrical conductivity.

Amborski investigated the structural dependence of the electrical conductivity of polyethylene terephthalate (117). Schultz developed a rate process theory of semiconduction in organic crystals (118). Winslow, Baker and Yager studied a series of pyrolytic derivatives and correlated composition, conductivity and odd electron concentration in polymer molecules (119).

One of the most complete investigations in the field of conducting polymers has been made by Pohl and coworkers (120-141). In the early nineteen sixties they reported on results for metal doped pyropolymers (120-122). Many measurement techniques were developed here and used in subsequent studies. In 1962 the highly conducting conjugated polymers were discussed in relation to pressure (123), ESR (124), and chemical structure (125,126). By the mid-sixties many general articles and reviews had brought this subject into great importance in the field of solid state and molecular chemistry (127-135). In recent years the investigations have concentrated on polyacene quinone radical polymers (136). In 1966 Rosen and Pohl suggested the possibility of hyperelectronic polarization to explain the high dielectric constants observed (1). The investigations concerning the actual bulk properties and existence of hyperelectronic polarization were carried out by Hartman and Pohl (137,138,3). This effect has also been observed recently by Jonscher and Chan (139) in the black carbon disulfide polymer. Recently Pohl has reviewed the structural parameters of various semiconducting polymers with emphasis on the effects of pressure (140). An excellent review, discussing the behavior of these polymers from a theoretical

standpoint, has been given by Pohl (141). The work by Pohl and cowork-
ers is briefly mentioned here in a historical context and will be dis-
cussed in detail later with reference to the present work.

Statement of the Problem

Hyperelectronic polarization has been shown by Hartman (3) to be a
real effect inherent in the bulk of the polymer sample. The problem
which now remains concerns the actual nature of the observed phenomenon.
It is important to recognize that the observation of this extreme polar-
ization occurs simultaneously with high conductivity in these polymeric
semiconductors. In attempting to explain any mechanism concerned with
hyperelectronic polarization one must also include the conducting
mechanisms.

The problem is now to carefully study the responses of the conduc-
tivity and permittivity to pressure, temperature and electric field fre-
quency and intensity. From these results clues are to be extracted to
determine which processes form the overall macroscopic effects. This
may be accomplished by developing usable empirical and theoretical ex-
pressions which will correctly describe the behavior observed. When
possible, the structural parameters, such as molecular length and mono-
mer units, will be compared to the electric responses, thus leading to a
more complete understanding of the polarization and related transport
mechanisms.

CHAPTER II

MATERIALS AND EXPERIMENTAL TECHNIQUE

Semiconducting Polymers

A great variety of organic compounds have been shown to exhibit
semiconduction. For purposes here the materials will be restricted to
those which conduct electronically rather than ionically. The general
subject is reviewed extensively by Gutmann and Lyons (142) and by Kanda
and Pohl (27).

The conductivity of conjugated polymers ranges from 10^{-16} mho/cm
for polynapthalenes to 10^4 mho/cm for pyropolymers. The conjugated
polymers have been separated into two groups by Pohl (141). The first
group, called rubiconjugated polymers, contains those polymers which
have interrupted regions of electron delocalization and are poor conduc-
tors with conductivities of less than 10^{-10} mho/cm. The second group,
called ekaconjugated polymers, contains those polymers which have long
continuous regions of delocalization and conductivities in the range of
10^{-9} to 10^4 mho/cm. A quantum mechanical explanation has been given by
Pohl (141). The polymers used in this study are of the second type.

In 1964 Little suggested the possibility of an organic superconduc-
tor (143,144). Since then many researchers have commented on the like-
lihood of a room temperature organic superconductor (145 - 156). The
study of conducting polymers has come into prominence in the search for
such a material. If the mechanism and structure of conducting polymers

can be determined, the search for an organic superconductor may be great-
ly enhanced.

The polyacene quinone radical polymers have been shown to exhibit
hyperelectronic polarization (1,3). A large variety of samples of this
type have been kindly prepared by Dr. J. Mason and have been extensively
used in this study.

Each polymer of this type was prepared by heating a mixture of pure
monomeric acene with pyromellitic dianhydride (PMA) or mellitic trianhy-
dride (MTA) with $ZnCl_2$ as a catalyst for a period of 24 hours at $295^{\circ}C$
under a nitrogen atmosphere. The mole ratio of acene : anhydride : cata-
lyst was 1 : 1 : 2. The resulting product, consisting of hard, black
polymer and non-reacted components, was first triturated with 1 per
cent hydrochloric acid and water to remove the $ZnCl_2$. Extraction for
24 hours with boiling ethanol and then boiling benzene in a Soxhlet ap-
paratus was done to remove all soluble impurities and unreacted acene
and anhydride. The remaining insoluble polymer was finely ground and
dried in a high vacuum over phosphorous pentoxide. A desiccator was
used to store the samples until measurement (136). The 29 samples pre-
pared by this technique and used in this study are listed in Table I.
The polymer samples will be referred to in the form Hydrocarbon-Acid;
for example, thianthrene-PMA.

Another anthroquinone-PMA sample was prepared in a similar manner
by D. Pohl. The reactants were heated to $300^{\circ}C$ for 24 hours in nitrogen
atmosphere. The sample was highly purified by extracting with toluene,
ethanol and benzene after being finely ground and leached with dilute
HCl. This sample is referred to as anthraquinone-PMA-HP.

A quinazone polymer was prepared by E. H. Engelhardt (126) by

TABLE I

COMPOSITION OF POLYMER SAMPLES
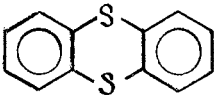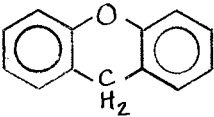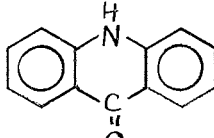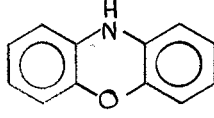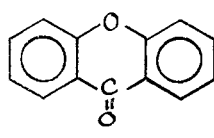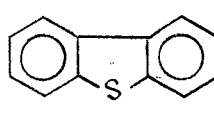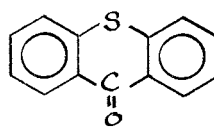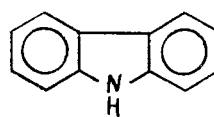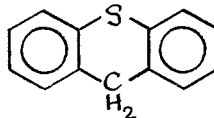
Code	Hydrocarbon Derivative Portion		Acid Portion
JM 39		Thianthrene	PMA
JM 40		Xanthene	PMA
JM 41		Acridone	PMA
JM 42		Phenoxazine	PMA
JM 43		Xanthone	PMA
JM 46		Dibenzothiophene	PMA
JM 48		9-Thioxanthane	PMA
JM 49		Carbazole	PMA
JM 50		9-Thioxanthene	PMA

TABLE I. (Continued)

Code	Hydrocarbon Derivative Portion		Acid Portion
JM 51		Thianthrene	MTA
JM 60		Anthrone	MTA
JM 61		Acridone	MTA
JM 62		Dibenzothiophene	MTA
JM 64		Xanthene	MTA
JM 65		Carbazole	MTA
JM 66		Acridine	MTA
JM 75		Fluorene	PMA
JM 76		9-Fluorenone	PMA
JM 77		Acridan	PMA
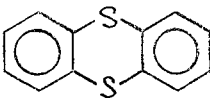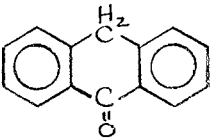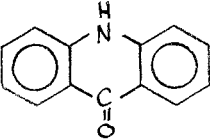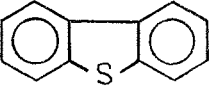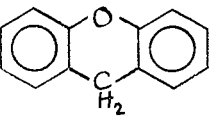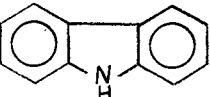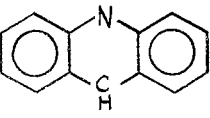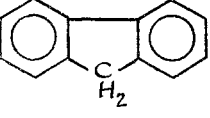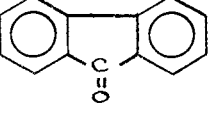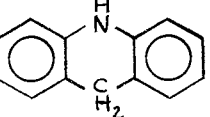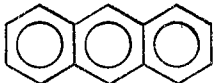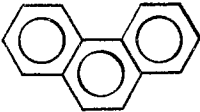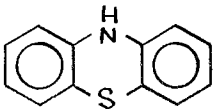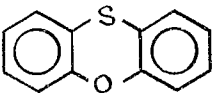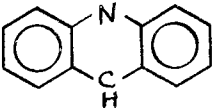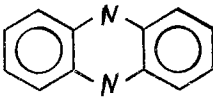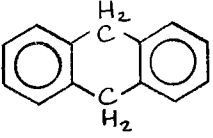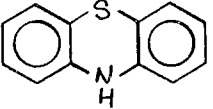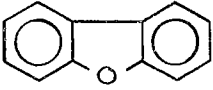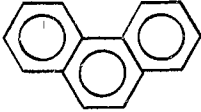
TABLE I. (Continued)

Code	Hydrocarbon Derivative Portion		Acid Portion
JM 77B		Anthracene	PMA
JM 78B		Phenanthrene	PMA
JM 80		Phenothiazene	PMA
JM 81		Phenoxathiin	PMA
JM 83A		Acridine	PMA
JM 84A		Phenazine	PMA
JM 85		9,10-Dihydroanthracene	PMA
JM 85A		Phenothiazene	PMA
JM 86		Dibenzofuran	PMA
JM 93B		Phenanthrene	MTA

reacting equimolar quantities of 1,4-naphthoquinone with p-tolune-diiso-
cyanate at 250°C for 15 minutes under a nitrogen atmosphere. The poly-
mer obtained was finely ground and exhaustively extracted with water,
ethanol and toluene in a Soxhlet apparatus. The purified polymer was
then dried and stored over a drying agent in a desiccator until used.
This sample is designated as 1,4-naphthoquinone-P-TODI.

A metallo-organic polymer was prepared by reacting equimolar quan-
tities of NN'-di(β-hydroxyethyl)-dithiooxamide dissolved in warm etha-
nol-water mixture with cupric acetate solution in ethanol as reported by
Kanda (157). A black precipitate formed rapidly upon mixing the solu-
tions. The mixture was let stand overnight, filtered, then extracted 72
hours with benzene, then 24 hours with alcohol, then 24 hours with water
in a Soxhlet apparatus. The polymer was then dried and stored in a des-
iccator. This polymer is designated as Cu-coordination polymer.

A set of pyropolymers was prepared by D. Litchinsky using the pro-
cedure described by Pohl and Rosen (122), using Amberlite ion exchange
resin IRC-84 as the starting material. The metal doped pyropolymers
were prepared by contacting the gently stirred ion exchange resin with
0, 0.15, 0.45, 1.5 and 4.5 $\underline{M}$ aqueous solutions of sodium, calcium or
nickel nitrate, for one week. The drained, rapidly rinsed polymers were
then dried, preoxidized at 300°C for several days, ground, then heat-
treated under helium atmosphere for two hours at 600°, 800° or 1000°C,
cooled and stored under dry nitrogen. The samples were coded according
to metal-doping and heat treatment. For example, pyropolymer 0.45 Ca-
600 has been doped using 0.45 $\underline{M}$ $Ca(NO_3)_2$ and heat-treated under helium
gas at 600°C for two hours.

High Pressure and Temperature Measurements

The high pressure cell used for conductivity and permittivity measurements is shown in Figure 1. The sample, which was first pressed into a pellet at low pressure, was then placed in a pyrophyllite ring between the two beveled tungsten carbide steel anvils. The sample was 3 millimeters in diameter and 0.20-0.30 millimeters in thickness. The anvil surface diameter and outer pyrophyllite ring diameter were 6 millimeters. Pyrophyllite has the property of exerting lateral pressure when squeezed vertically. Although the anvils exerted uniaxial pressure on the sample, it was contained by the pyrophyllite ring. Copper shims were placed between the anvils and steel blocks to prevent the anvils from cracking when the pressure was applied. Copper electrodes were placed between the insulating material and the back-up blocks. A cylinder of Teflon was placed between the anvils and steel jacket for electrical insulation. A copper-constantin thermocouple was placed on the anvil near the sample.

The high pressure cell was placed between the platens of a Passadena Hydraulic Press Model SB230C. The press is capable of producing a load of 50 tons, but the load was restricted to 14 tons to prevent the anvils from "cupping" or pitting. This load produced a pressure of 44 kilobars on the sample. The samples were initially exposed to this pressure, and the measurements were made for pressures up to 32 kilobars. The press had been previously calibrated by Hartman (3), using a strain guage. After a sample had been subjected to high pressure (44 kbars), the results (conduction and permittivity data) were reproducible for all lower pressures.

The sample could be heated by thermostatically controlled heating
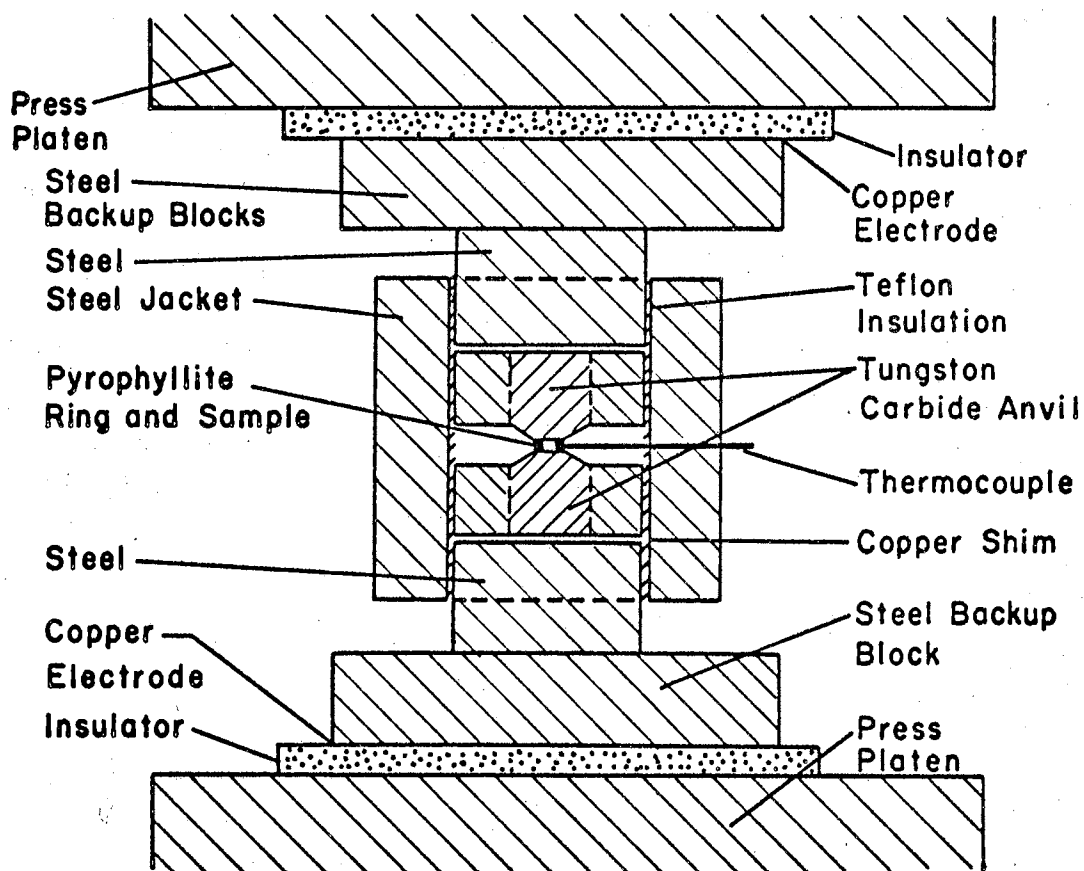
Figure 1. Diagram of the High Pressure Cell Used for Conductivity
and Permittivity Measurements

elements in the press platens. The maximum temperature of the sample was limited to 110°C to protect the sample from degradation and to prevent softening of the Teflon insulation. A period of at least 2 hours was necessary between measurements to allow the press platens, high pressure cell and sample to come to equilibrium, since the thermocouple was not in actual contact with the sample.

Direct current conductivity measurements were made using a Keithley 610B electrometer in the resistance mode. The electric field intensity was restricted to low values so that the field effect was negligible. This limiting value depended upon the sample conductivity and will be discussed later. Using this technique, samples with in-place resistances of $10^3 - 10^{11}$ ohms could be measured.

A Koops (158) type impedance comparison bridge was used to measure the a. c. conductivity and permittivity. The bridge basically compares an unknown impedance against a known standard impedance. The unknown or sample impedance was modelled as a capacitor and resistor in parallel, and was thus compared to a known standard capacitor and resistor in parallel. The actual bridge circuit, shown in Figure 2, employed a General Radio 716C capacitance bridge. A bridge balance was achieved when the null detection system showed no signal. This was accomplished by simultaneously adjusting the standard resistor to balance the in-phase impedance, and the standard capacitor to balance the out-of-phase impedance of the sample. The values of the standard resistor and capacitor were thus the in-place resistance of the sample and the total system capacitance of sample, high pressure cell, leads and bridge.

The sample capacitance was calculated by taking the difference between the total capacitance with the sample in place and with the sample
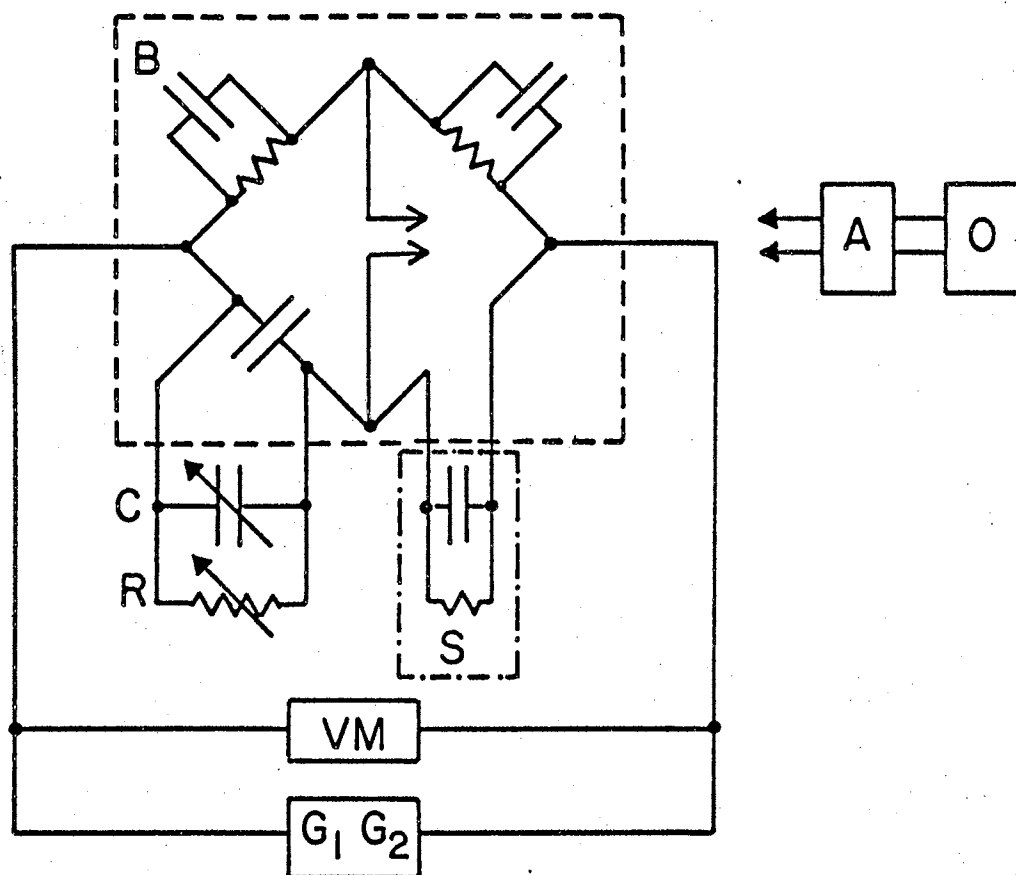
O - Hewlett-Packard Model 130C Oscilloscope
A - General Radio Type 1232-A Tuned Amplifier and Null Detector
G_1 - Hewlett-Packard Model 200 CD Wide Range Oscillator
G_2 - Hewlett-Packard Model 205 AG Audio Signal Generator
B - General Radio Type 716-C Capacitance Bridge
VM - Hewlett-Packard Model 400 AD Vacuum Tube Voltmeter
R - General Radio Type 1434-G Decade Resistance
C - General Radio Type 1412-BC Decade Capacitance
S - Sample

Figure 2.   Diagram of the Bridge Circuit for A. C. Conductivity
and Permittivity Measurements

removed. This was easily done since the pyrophyllite ring maintained the anvil gap and allowed air to replace the sample. The system's intrinsic capacitance was then determined as a function of frequency. The capacitance of each decade of the standard resistor was also determined for the entire frequency range. Several thicknesses of mica and Teflon were placed in the sample position and the capacitances were determined for each configuration. No measurable change in the intrinsic system capacitance was observed for anvil separations of 0.20 to 0.30 millimeters.

For pressure, temperature and frequency effect investigations the field intensity in the sample was limited in the same manner as in the d. c. conductivity case. The usable frequencies were limited to the range of 30 Hz to 300 kHz. The parallel mode method was limited to 1 megohm of sample resitance. Although most samples exhibiting hyperelectronic polarization were within this limit, it was sometimes necessary to use the series mode, which was the normal method for the General Radio 716C bridge. This technique is described in the operation manual.

The general method of pressure effect measurements employed either the d. c. conductivity circuit or the a. c. impedance bridge. The sample pellet was placed in the high pressure cell and squeezed to the maximum pressure, 44 kilobars. This eliminated voids and particle interfaces.

In a study by Hartman (3) the sample was measured after high pressure premolding. Another sample of the same polymer was sheared under pressure and then placed in the high pressure cell and measured under the same conditions. The results were the same and it was concluded that all voids were removed by high pressure premolding. In that same

study several electrode materials were used, including gold and plati-
num. The results were the same as those for the tungsten carbide steel
electrodes. It was concluded that the pressure, temperature and fre-
quency effects were due to the bulk properties of the material.

In this investigation, after initial premolding at 44 kilobars,
the pressure was slowly lowered to the lowest pressure, 3 kilobars. If
the temperature of the system was in equilibrium, the d. c. resistance
was determined or the impedance bridge was balanced. Measurements were
then taken at four or five more pressures, up to 32 kilobars, in a simi-
lar manner. From these results the pressure coefficients for conduction
and permittivity were determined.

The conduction or permittivity activation energy was determined by
heating the sample to the highest temperature, $110^{\circ}C$, and allowing the
system to reach equilibrium. The resistance and permittivity measure-
ments were made for the selected pressures between 3 and 32 kilobars.
The temperature was then lowered and the measurements repeated. As the
press platens were water cooled, the lowest temperature was normally
$20^{\circ}C$. From these results the activation energies could be obtained as
a function of pressure.

Electric Field Intensity and Frequency Effects

The d. c. field effect measurements are used to observe small de-
viations in Ohm's law. Using various techniques, this effect has been
measured for polyacene quinone radical samples by Rosen and Pohl (1) and
by Hartman (3). A method for determining the molecular length from the
results has been developed (1).

The method used in this investigation has been shown to give

excellent results with a wide range of field intensities. The circuit, a Wheatstone Bridge, is shown in Figure 3. The voltage supply circuits are shown in Figure 4. Using the proper components, one can measure the field effect of samples with in-place resistances ranging from 10^2 to 10^{10} ohms. The lower limit was due to the 0.1 ohm limit of the standard decade resistance S. The upper limit was due to the lack of sufficient current to produce a deflection on the galvanometer (10^{-11} amperes/mm).

Since the purpose of these measurements was to determine the molecular length, these measurements could be made at any constant temperature and constant pressure. Thus in this investigation these parameters were used to produce convenient sample resistances and also to check and reproduce the results. In practice it was noticed that the results remained constant for low pressure (3-7 kilobars) measurements, but that the effect increased for very high pressure (20-30 kilobars). This may have been due to the increase in conductivity which in turn would increase the probability of Joule heating at higher field intensities. The measurements were taken at room temperature.

If the sample resistance X was less than 10^6 ohms, the ratio arms of the bridge, A and B, were set equal at approximately the value of the standard resistance S when the galvanometer produced a null. This value was recorded along with the voltage reading of the volt meter VM. This value was twice the voltage drop across the sample since half the total voltage was dropped in the standard resistance S.

For sample resistances greater than 10^6 ohms, resistance A was set at 10^5 ohms and resistance B' was used in place of B. The resistance B' was set at 10^7 ohms or greater, depending on the sample resistance. The
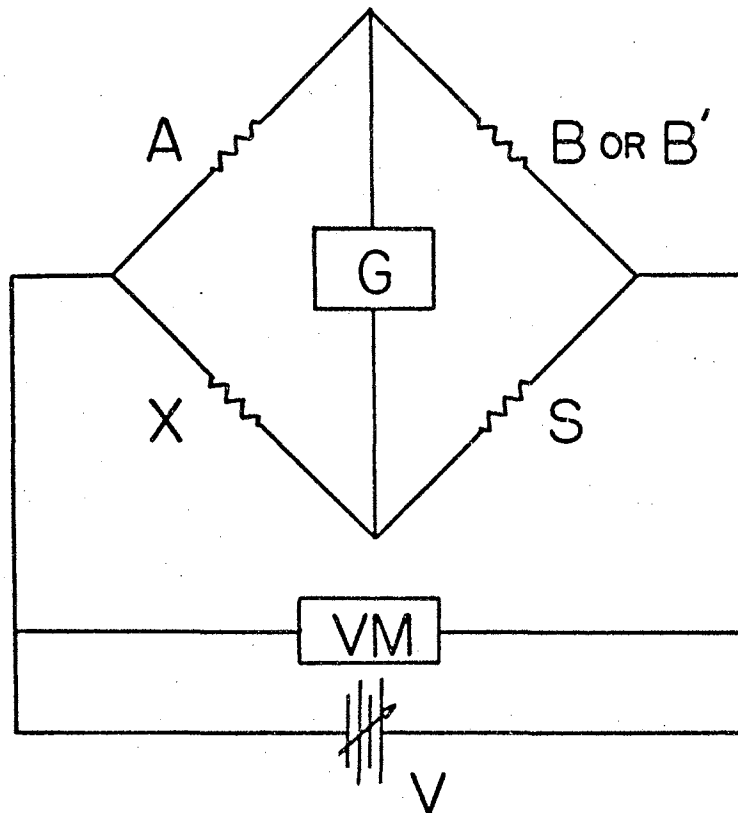
A,B = Heathkit Model IN-11 Decade Resistance
        $(1-10^6$ ohm)
B' = Keithley Model 2008 Decade Shunt
        $(10^6-10^{12}$ ohm)
G = Leeds and Northrup Model 2430-C Galva-
        nometer
X = Sample
S = General Radio Type 1434-G Decade
        Resistance $(0.1-10^6$ ohm)
VM = Keithley Model 610B Electrometer
        (0.001-100v.d.c.) or RCA WV-9A Senior
        Voltohmyst (100-2000v.d.c.)
V = Power Supply, as Shown in Figure 4.

Figure 3. Diagram of Bridge Circuit for D. C.
            Field Effect Measurements

0.001-2.0 V R S B

2-35 V R PS1

35-500 V PS2

500-2000 V PS3
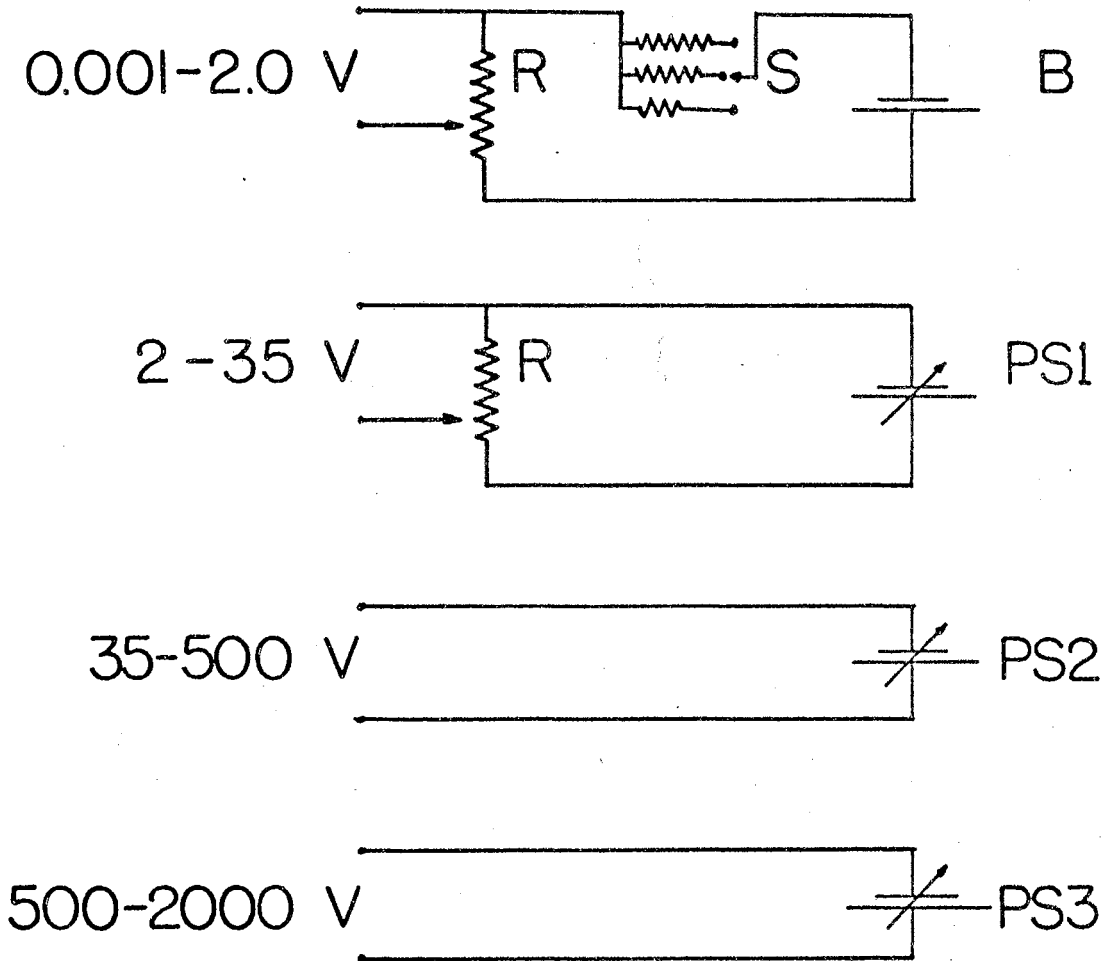
R   – 4200 Ohm Variable Power Resistor
S   – Keithley Model 2008 Decade Shunt (10^6–10^{12} ohm)
B   – One 2-Volt Cell of a 6-Volt Storage Battery
PS1 – Heathkit Model EUN-17 Transistorized Power Supply
PS2 – Heathkit Model PS-3 Variable Voltage Regulated Power Supply
PS3 – Hamner Model N401 High Voltage Power Supply

Figure 4.   Diagram Showing the Four Power Supplies Used for the
          D. C. Field Effect Measurements

The bridge was balanced by adjusting the standard resistance S. The re-sistance value was then multiplied by the ratio B'/A to obtain the sam-ple resistance. Sensitivity was lost by that ratio and thus higher voltages were necessary. For the case of B'/A = 100, the voltage drop across the sample was the value read on the volt meter, since 99 per cent of the total voltage was dropped across the sample.

The field intensity $\mathcal{E}$ is calculated from the voltage drop across the sample, V, and the sample thickness, which were measured after the conductivity measurements were made. In the high pressure cell the sam-ple thickness t was 0.20-0.30 millimeters. The field intensity $\mathcal{E}$ in units of volts/cm was determined by the expression

$$\mathcal{E} = \frac{10V}{t} \text{ volts/cm}.$$ (1)

From the theory of electric field effect developed by Rosen and Pohl (1), the ratio of the conductivity at a finite field to the con-ductivity at zero field is given by

$$\frac{\sigma}{\sigma_o} = \frac{2kT}{|e|\mathcal{E}L} \left[e^{\frac{|e|\mathcal{E}L}{2kT}} - 1 \right]$$ (2)

where k is Boltzmann's constant, T is the absolute temperature, e is the electronic charge, and L is the molecular length. If one sets $x = |e|\mathcal{E}L/2kT$, then equation (2) becomes

$$\frac{\sigma}{\sigma_o} = \frac{1}{x} (e^x - 1).$$ (3)

Expanding e^x in the familiar series expansion and substituting into equation (3),

$$\frac{\sigma}{\sigma_o} \cong \frac{1}{x} \left[1 + x + \frac{x^2}{2!} + \frac{x^3}{3!} + \cdots - 1 \right].$$ (4)

And for small values of $\mathcal{E}$ (low field intensities),

$$\frac{\sigma}{\sigma_o} \cong (1 + \frac{x}{2})$$

$$\cong 1 + \frac{|e|\mathcal{E}L}{4kT} .$$

(5)

A thermal field effect may also arise due to the change in conductivity when heat is dissipated by an electric field across the sample. The electric field effect due to molecular length will be ignored here, since the effective magnitude of each effect will be the ultimate result.

The conductivity at temperature T_1 is given by

$$\sigma_1 = \sigma_\infty \exp \left[- \frac{E_a}{kT_1} \right] ,$$

(6)

and at temperature T_2 is given by

$$\sigma_2 = \sigma_\infty \exp \left[- \frac{E_a}{kT_2} \right]$$

(7)

where σ_∞ is the conductivity at infinite temperature, E_a is the thermal activation energy and k is Boltzmann's constant. Then dividing equation (6) by equation (7),

$$\frac{\sigma_1}{\sigma_2} = \exp \left[- \frac{E_a}{k} \left(\frac{1}{T_1} - \frac{1}{T_2} \right) \right]$$

$$= \exp \left[- \frac{E_a}{k} \left(\frac{T_2 - T_1}{T_1 T_2} \right) \right] .$$

(8)

If one sets $\Delta T = T_2 - T_1$, and $T = T_1 = T_2 - \Delta T$, then

$$\frac{\sigma_1}{\sigma_2} = \exp \left[- \frac{E_a}{k} \left(\frac{\Delta T}{T (T + \Delta T)} \right) \right] .$$

(9)

If $\Delta T \ll T$, then $T(\Delta T + T) \cong T^2$ and

$$\frac{\sigma_1}{\sigma_2} = \exp\left[-\frac{E_a}{k}\left(\frac{\Delta T}{T^2}\right)\right] . \tag{10}$$

Expanding the exponential term as was done in equation (4), then for

$$\frac{\sigma_2}{\sigma_1} = \exp\left[\frac{E_a}{k}\left(\frac{\Delta T}{T^2}\right)\right] \tag{11}$$

one has

$$\frac{\sigma_2}{\sigma_1} = 1 + \frac{E_a}{k}\left(\frac{\Delta T}{T^2}\right) . \tag{12}$$

The magnitude of the second term on the right side of equation (12) can be determined if the value of ΔT is calculated. It is suggested here that the change in temperature is due to the heat dissipated in the sample when an electric field is placed across the sample. For purposes of simplification one can assume the heat produced in the sample is produced at the center of the sample. The temperature of the anvils is T_1 and the temperature of the center of the sample is T_2. For equilibrium conditions the power produced is related to the temperature difference for one half the sample by

$$\dot{Q}_{t/2} = \frac{c \cdot A \cdot \Delta T}{(t/2)} \tag{13}$$

where $\dot{Q}_{t/2}$ is the power dissipated, c is the coefficient of heat conductivity, and A is the cross-sectional area of the sample. But the heat is conducted away from the center in two directions; thus,

$$\dot{Q} = 2\dot{Q}_{t/2} = \frac{4c \cdot A \cdot \Delta T}{t} , \tag{14}$$

and

$$\Delta T = \frac{\dot{Q}}{4} \left(\frac{t}{A}\right)\left(\frac{1}{c}\right) \quad .$$

(15)

The power dissipated in the sample is related to the field intensity by the expression

$$\dot{Q} = \mathcal{E}^2 t A \sigma \quad .$$

(16)

Then the change in temperature is related to the field by

$$\Delta T = \mathcal{E}^2 t^2 \sigma / c$$

(17)

where $\mathcal{E}$ is the electric field intensity. Then substituting equation (17) into equation (12),

$$\frac{\sigma_2}{\sigma_1} \cong 1 + \left(\frac{E_a t^2 \sigma}{c k T^2}\right)\mathcal{E}^2 \quad .$$

(18)

By inserting the typical values for the terms in equation (18), the magnitude of the heating effect can be estimated. Let

$t = 0.25$ cm

$t^2 = 0.000645$ cm^2

$k = 0.8617 \times 10^{-4}$ eV/$^\circ$K

$c = 12 \times 10^{-4}$ watts/cm$^\circ$K

$T = 300^\circ$K

$T^2 = 9 \times 10^4$ $(^\circ K)^2$.

Then

$$\frac{\sigma_2}{\sigma_1} = 1 + 6.63 \times 10^{-2} E_a \sigma \mathcal{E}^2 \quad .$$

(19)

Then for typical values of the conductivity, $\sigma = 10^{-4}$ mho/cm, and the

activation energy, $E_a = 0.2$ eV, an electric field intensity of 87 volts/ cm would cause a one per cent change in the conductivity. Equation (19) indicates that the Joule heating effect is approximately a function of the square of the field intensity, while equation (5) suggests that the molecular length field effect is approximately a linear function of the field intensity. If one assumes that these two effects are predominant for these samples and measurement conditions, then the results can be analyzed accordingly.

The a. c. field effect measurements used the previously described impedance bridge shown in Figure 2. Here the rms input voltage was measured using a Hewlett-Packard 200CD A. C. Voltmeter. The voltage was also checked with a Hewlett-Packard Model 203A Wave Analyzer, since several different frequencies were used. When the bridge was balanced in the parallel mode, the meter voltage was twice the rms voltage across the sample. The rms field intensity was determined in the same manner as equation (1). A similar technique was used by Rosen and Pohl (1) and by Hartman (3). Rosen and Pohl developed a technique to determine the proper wave form of the detection signal to account for the field effect within the sinusoidal response. An absolute null could not be achieved since the capacitance and resistance of the sample changed with applied voltage. This technique included the d. c. molecular length field effect for conductivity, but did not permit quantitative molecular length results.

Joule heating was also to be considered for highly conductive samples. The maximum voltage output of the oscillator was 96 rms, and thus only 48 volts could be applied to the sample. Most of the samples measured did not show any effects of heating.

Electron Spin Resonance

The electron spin resonance measurements were used as one method of determining the molecular length of the molecules. This method was suggested by Pohl (141) and has been used by Hartman (3).

The molecule is modeled as a quantum mechanical box containing the unpaired spins which can be thermally activated. The separation of the energy levels is proportional to the length of the box, which is the length of the molecule. The spin activation energy is the energy required to raise an electron from the highest occupied molecular orbital (HOMO) to the lowest empty molecular orbital (LEMO), and if the unpairing energy is assumed to be small, then the free electron approximation is used. Then

$$E_\beta = \frac{h^2}{4 m l_o z}$$

(20)

where $L = l_o z$, h is Planck's constant, m is the mass of the electron, l_o is the C-C bond length and z is the number of C-C bonds in a linear segment.

The number of spins/gram for each sample was determined by comparing the measured susceptibility χ of the sample to that of a known standard, DPPH. As the resonance signal for the samples was much broader than the DPPH signal, a secondary or intermediate standard was calibrated and the number of spins determined for each temperature. The details of calibration and operation of the Alpha Scientific Laboratory Model AL 340 SY Electron Spin Spectrometer have been reviewed by Hartman (3). The powder samples were first outgassed to remove water and any oxygen present.

The number of spins, the Curie point, and the spin activation energy

were determined by measuring the susceptibility at three well-defined temperatures: room temperature ($296°K$), dry ice temperature ($194°K$) and liquid nitrogen temperature ($77°K$). From the Curie-Weiss law, the susceptibility is given by,

$$\chi = \frac{S \, g^2 \beta^2}{4 \, k \, (T - \Theta)} \qquad (21)$$

where g is the Lande factor, β is the Bohr magneton, S is the number of unpaired spins, k is Boltzmann's constant, T is the temperature and Θ is the Curie point. For an activated process,

$$S = S_0 \exp\left[-\frac{E_S}{kT}\right] \qquad (22)$$

where S_0 is the number of spins at $T = \infty$, and E_S is the spin activation energy. For the standard, DPPH, there is no activation energy or Curie point. Thus

$$\chi_{DPPH} = \frac{S_{0DPPH} \, g^2 \beta^2}{4 \, k \, T} \qquad (23)$$

Then taking the ratio of the two susceptibilities,

$$R = \frac{\chi}{\chi_{DPPH}} = \frac{S_0}{S_{0DPPH}} \exp\left[-\frac{E_S}{kT}\right]\left(\frac{T}{T - \Theta}\right) . \qquad (24)$$

Then for the three temperatures, T_1, T_2, T_3:

$$\frac{R_1}{R_2} = \exp\left[-\frac{E_S}{k}\left(\frac{1}{T_1} - \frac{1}{T_2}\right)\right]\left(\frac{T_1 \, (T_2 - \Theta)}{T_2 \, (T_1 - \Theta)}\right) ,$$

and

$$\frac{R_1}{R_3} = \exp\left[-\frac{E_g}{k}\left(\frac{1}{T_1} - \frac{1}{T_2}\right)\right]\left(\frac{T_1 \ (T_3 - \oplus)}{T_2 \ (T_2 - \oplus)}\right). \tag{26}$$

The two equations (25) and (26) contain two unknowns, E_g and $\oplus$, and were solved by iteration on a computer.

The data obtained with the assistance of R. Franklin was analyzed using the above method. The results and molecular lengths are given in Table II. These results will be compared and discussed in Chapter III. An error analysis was performed to check the reproducibility for this spectrometer. Table III shows the susceptibility ratios of the secondary standard to the primary standard DPPH for the temperatures used. This essentially shows the reproducibility of the number of spins for any particular measurement. There was a consistant 12.5 per cent standard deviation from the average value.

X-Ray Diffraction Studies

X-ray diffraction patterns were obtained for several types of semiconducting polymers. The purpose was to obtain information about the inter-planar and other observed spacings of polymers which have been studied from the electronic aspects.

The forward-reflection or transmission technique was used as it is recommended for amorphous materials when diffusion is present. The various techniques for x-ray diffraction have been discussed in detail (159, 160), giving the advantages and disadvantages of each method (161). The samples were measured using a General Electric apparatus with a CA-7 x-ray tube. The target material was copper, producing a wavelength of

TABLE II.

ELECTRON SPIN RESONANCE RESULTS: ACTIVATION ENERGY,
CURIE POINT AND MOLECULAR LENGTH

Sample	E_s (eV)	$\Theta(^\circ K)$	L (Å)
Thianthrene-PMA	0.0138	50.1	3359
Xanthene-PMA	0.0270	68.3	1721
Acridone-PMA	0.0344	74.4	1352
Phenoxazine-PMA	0.0108	49.9	4322
Xanthone-PMA	0.0360	73.0	1292
Dibenzothiophene-PMA	0.0374	75.2	1243
9-Thioxanthene-PMA	0.0234	61.2	1984
Fluorene-PMA	0.0187	45.9	2482
9-Fluorenone-PMA	0.0553	76.6	841
Acridan-PMA	0.0450	75.8	1031
Anthracene-PMA	0.0106	29.7	4369
Phenothiazene-PMA	0.0662	76.9	702
Phenoxathiin-PMA	0.0463	76.6	1003
9,10-Dihydroanthracene-PMA	0.0489	76.3	951
Phenothiazene-PMA	0.0317	72.5	1465
Dibenzofuran-PMA	0.0398	75.5	1168
9-Thioxanthane-PMA	0.0249	69.1	1866
Carbazole-PMA	0.0328	70.3	1415

TABLE III.

THE RATIOS OF SUSCEPTIBILITIES OF THE SECONDARY
STANDARD TO THE DPPH #2

Run #	77°K	194°K	296°K
6	0.37	0.30	0.30
7	0.28	0.29	0.25
8	0.35	0.33	0.34
9	0.37	0.27	0.26
10	0.27	0.35	0.32
11	0.37	0.36	0.37
12	0.31	0.39	0.31

1.54 ångstroms. The compressed powder sample was placed in front of the collimated x-ray beam. The flat-film camera was placed 0.041 m from the sample. The lead shield helped to absorb the scattered x-rays.

For each sample picture the film was exposed for 15 minutes with the plate voltage set at 45,000 volts and the filament current at 0.015 amps. The Bragg angle $\ominus$ was determined by the expression,

$$2\ominus = \tan^{-1}\left(\frac{r}{D'}\right) \tag{27}$$

where r is the radius of the ring and D' is the distance between the sample and the film. The Bragg or inter-planar distance d was calculated from the Bragg law,

$$d = \frac{\lambda}{2} \cdot \frac{1}{\sin\ominus} , \tag{28}$$

where λ is the wavelength of the radiation.

Since most of the samples produced some diffusion of the rings, a rough calculation of the crystallite size was made using a Scherrer (161) relation,

$$D = \frac{K\lambda}{\beta \cos\Theta} \qquad\qquad (29)$$

where D is the crystallite dimension, λ is the x-ray wavelength, Θ is the Bragg angle, $K = 1$, and β is the dispersion angle. If the geometry of the crystallites is known, the parameter K can be determined more exactly. The results for the samples measured are given in Table IV, including powdered graphite for comparison purposes. The crystallite size indicates the amount of disorder or crystallinity. All of the samples have the same nearest neighbor distance of 3.4 angstroms, except for the Cu-coordination polymer.

TABLE IV

X-RAY DIFFRACTION RESULTS GIVING RANGE OF DISTANCES FOR HIGH
INTENSITY RINGS AND DISTANCES FOR LOW INTENSITY RINGS.
THE ROUGH ESTIMATE OF THE CRYSTALLITE DIMENSIONS
DUE TO RANGE OF HIGH INTENSITY RINGS

Sample	High Intensity ($\mathring{A}$)	Low Intensity ($\mathring{A}$)	D ($\mathring{A}$)
Graphite (powdered)	3.37 - 3.65 2.05 - 2.11	1.83, 2.20, 2.32, 2.68, 3.92, 4.72	90
Anthraquinone-PMA-HP	3.37 - 3.80	--	60
Thianthrene-PMA	3.42 - 4.23	--	36
1,4-Naphthoquinone- P-TODI	3.42 - 4.57 5.67 - 6.29	--	27 110
Cu-coordination Polymer	3.93 - 4.18 8.18 - 11.6	1.93, 2.85, 3.14, 3.39	130 55

CHAPTER III

RESULTS AND DISCUSSION

Pressure Effects

The effect of pressure on the d. c. conductivity of semiconducting polymers has been extensively studied (123,136,140). The concern here is the a. c. conductivity and permittivity pressure effect. Both the d. c. and a. c. pressure effects support a hopping mechanism rather than a band model. Comparison of the results will lead to the model for hyperelectronic polarization.

Pohl, Rembaum and Henry (123) have developed relations to explain the effect using the theory of absolute reaction rates. The electron transfers from one molecule to another by a hopping mechanism. If the pressure were increased, the orbital overlap between neighboring molecules would increase, thus increasing the rate of electron transfer. This rate or probability of transfer is directly related to the mobility. From an energy standpoint there is a barrier between the molecules, which can be referred to as the saddle height energy, E_s. The energy required for the formation of carriers, normally by a thermal means, is called the activation energy, E_a. This energy will also be affected by the orbital overlap between molecules.

In order to apply this theory to the a. c. conduction and permittivity, new notation must be made. The equation obtained by Pohl,

$$\ln\left(\frac{\sigma}{\sigma_o}\right) = P^{\frac{1}{2}}\left(\frac{b_o}{kT} + \frac{b''}{k}\right) = \left(\frac{b^*}{k}\right)P^{\frac{1}{2}} , \tag{1}$$

relates the change in conductivity, σ/σ_o , to the pressure P , where k
is Boltzmann's constant, T is the temperature, b_o is the pressure co-
efficient for the activation energy or enthalpy factor, b'' is the co-
efficient of pressure for the mobility or the entropy factor, and b^* is
the total pressure coefficient. The new notation equates b_o to b_E, b''
to b_S and b^* to b_T. The new notation must also be expanded to in-
clude the a. c. conductivity and permittivity effects. For simplicity,
a superscript is added to denote conduction or permittivity, b^σ and b^ϵ
respectively. The term is subscripted again to denote a. c. or d. c.
coefficients, $(b)_{AC}$ and $(b)_{DC}$ respectively.

Now equation (1) can be rewritten in the new notation as

$$\ln\left(\frac{\sigma}{\sigma_o}\right) = P^{\frac{1}{2}}\left(\frac{b_E^\sigma}{kT} + \frac{b_S^\sigma}{k}\right) = \left(\frac{b_T^\sigma}{k}\right)P^{\frac{1}{2}} , \tag{2}$$

and for the permittivity case,

$$\ln\left(\frac{\epsilon_r}{\epsilon_{ro}}\right) = P^{\frac{1}{2}}\left(\frac{b_E^\epsilon}{kT} + \frac{b_S^\epsilon}{k}\right) = \left(\frac{b_T^\epsilon}{k}\right)P^{\frac{1}{2}} . \tag{3}$$

From the results of Pohl, Rembaum and Henry (123),

$$E_a = E_{ao} - b_E P^{\frac{1}{2}} \tag{4}$$

where E_{ao} is the activation energy at zero pressure. Solving equation
(4) for b_E ,

$$b_E = (E_{ao} - E_a) / P^{\frac{1}{2}} . \tag{5}$$

Thus b_E is the slope of line for a plot of E_a vs $P^{\frac{1}{2}}$.

The value of b_s is then calculated from the expression

$$b_s = b_T - \frac{b_E}{T} \tag{6}$$

where b_T is the total pressure coefficient at temperature T. From these equations (5)(6), it is noticed that b_s and b_T are temperature dependent. In the investigation reported by Pohl (123) the values of b_s and b_T changed in the order of 10 per cent over the temperature range from $25^{\circ}C$ to $105^{\circ}C$. These differences are also of the order of experimental error and thus cannot be usefully associated with a particular mechanism.

The pressure effect data was obtained as a function of temperature and frequency by the technique described in Chapter II. The energy interval ΔE for carrier formation was calculated from the expression

$$\ln\left(\frac{\sigma_1}{\sigma_2}\right) = -\frac{\Delta E}{k}\left(\frac{1}{T_1} - \frac{1}{T_2}\right) \tag{7}$$

where σ_1 is the conductivity at temperature T_1 and σ_2 is the conductivity at temperature T_2, and k is Boltzmann's constant. This energy interval is the sum of the thermal activation energy for creation of carriers and the saddle-height energy of the thermally activated mobility process (140).

Typical results are shown in Figure 5. The permittivity ϵ_r and conductivity σ values are plotted as a function of 1000/T at a pressure of 6.3 kbars.

Figure 6 shows the reduced results for the xanthene-MTA polymer. The energy interval for conductivity and permittivity is plotted as a function of the square root of pressure. The slopes of the lines are
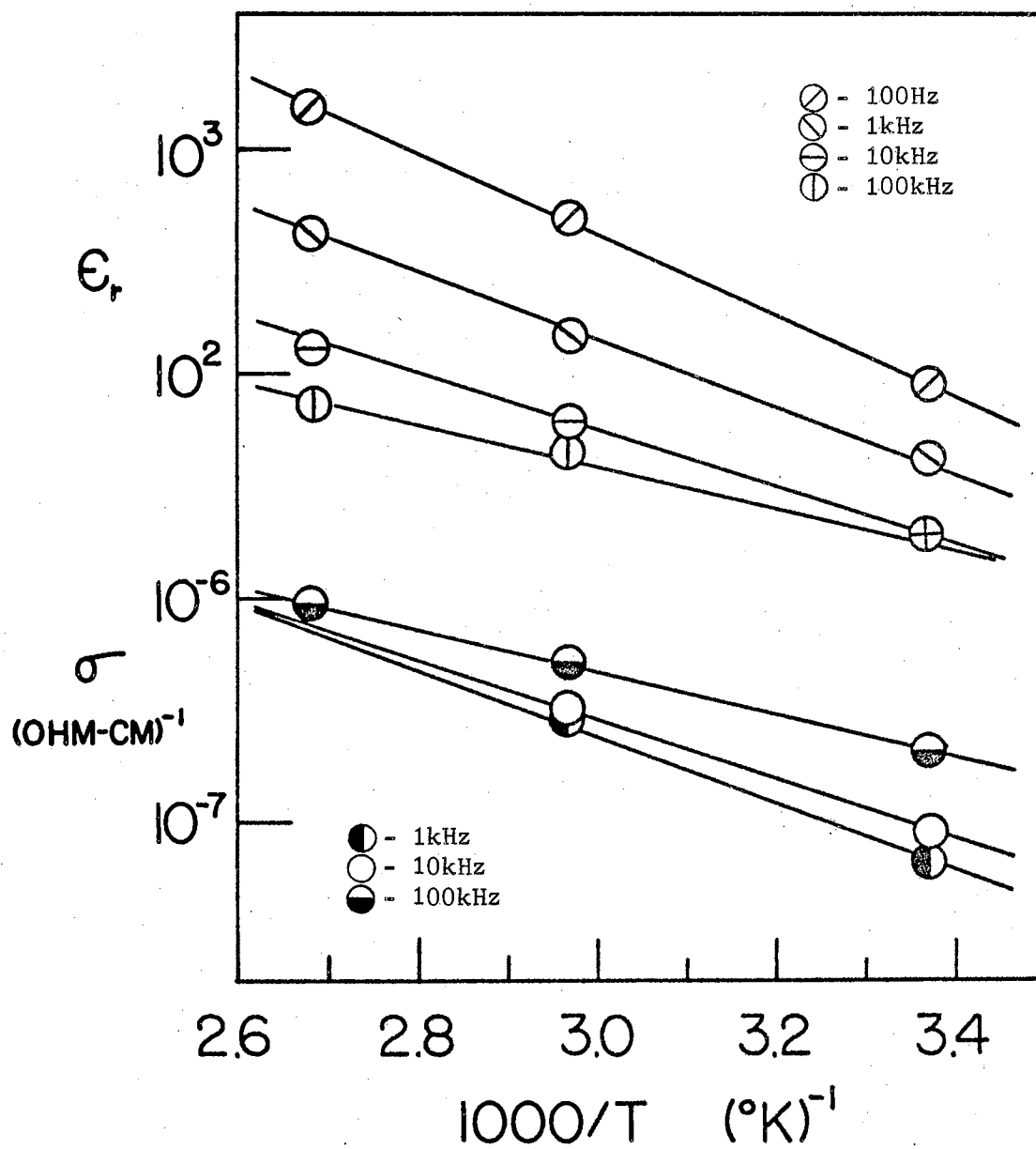
Figure 5. The Permittivity ϵ_r and the Conductivity σ as a Function
of 1000/T for the Xanthene-MTA Polymer at a Pressure of
6.3 Kilobars
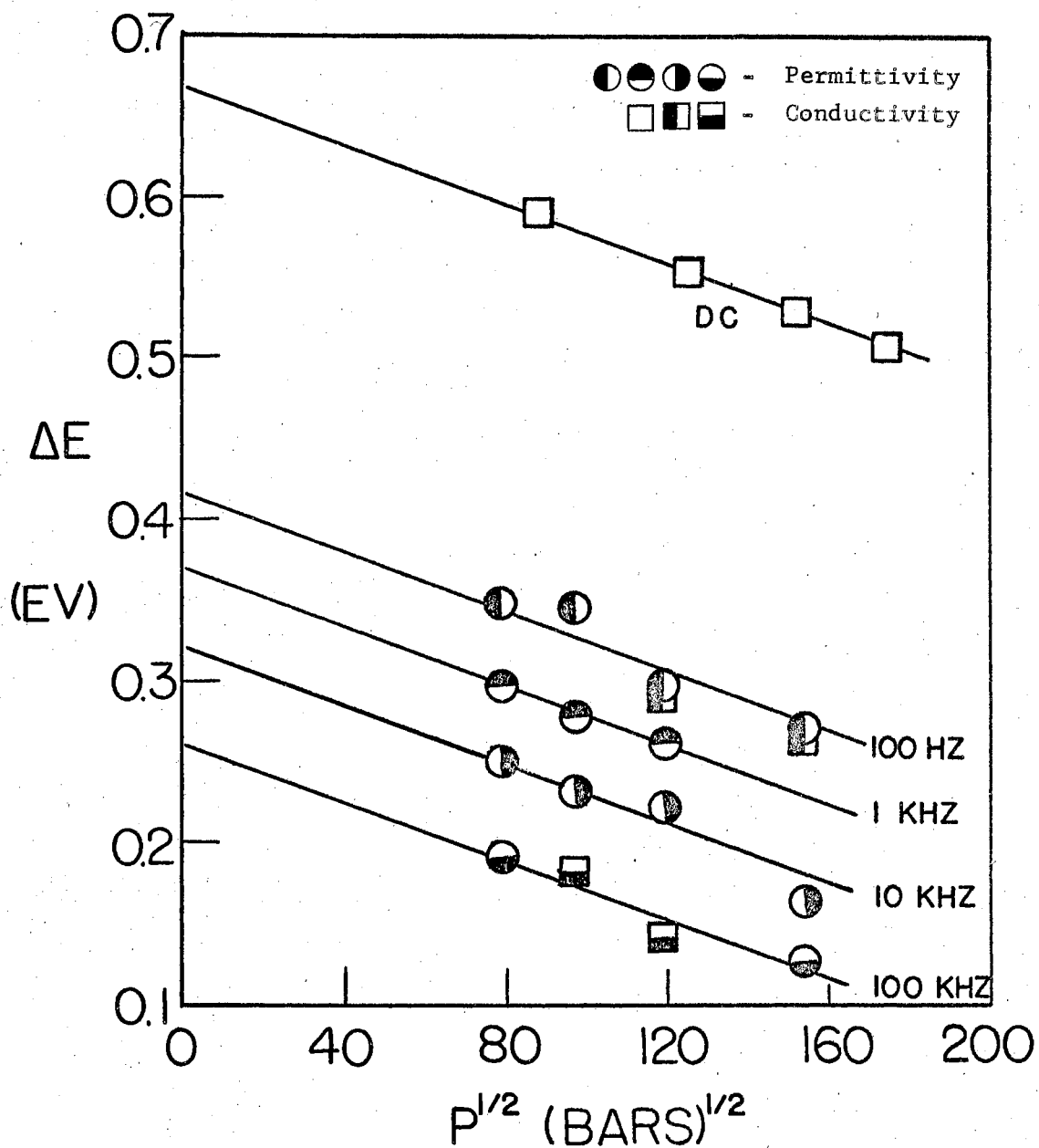
Figure 6. The Energy Interval, ΔE, as a Function of the Square Root of Pressure for the Xanthene-MTA Polymer

the values of b_E . The energy interval for the d. c. conductivity is much higher than for the a. c. conductivity or permittivity. The energy intervals for the permittivity and the conductivity are essentially the same. This suggests that the carriers and polarizing monopoles are ac-tivated by the same process. The decrease in energy interval with in-creasing frequency is consistent with the hopping model as described by Pollak (162). He suggests that the frequency dependence is weakened at higher temperatures due to multiple hops. This would decrease the change in conductivity with temperature at higher frequencies and thus decrease the thermal activation energy. Although the energy interval decreases with frequency, the activation energy pressure coefficient re-mains constant.

Figure 7 shows the results for another polymer which has a smaller energy interval and higher conductivity. The a. c. and d. c. conductiv-ity energy intervals are not as different as those of the preceeding sample and the frequency dependency cannot be distinguished. The value of b_E is the same for a. c. or d. c. conduction.

The results for the total conductivity pressure coefficient at room temperature are shown in Table V. The d. c. value is again less than the a. c. values, as expected for an a. c. hopping mechanism. There is a general decrease in the coefficient as the frequency increas-es. Since the value of b_E is essentially constant with frequency, the decrease must be due to a decrease in the entropy term, b_S , as the frequency increases. At lower frequencies the change in pressure more strongly aides the electron transfer process between molecules.

Table VI gives similar results for the total permittivity pres-sure coefficient, b_T , at room temperature for the same samples. The
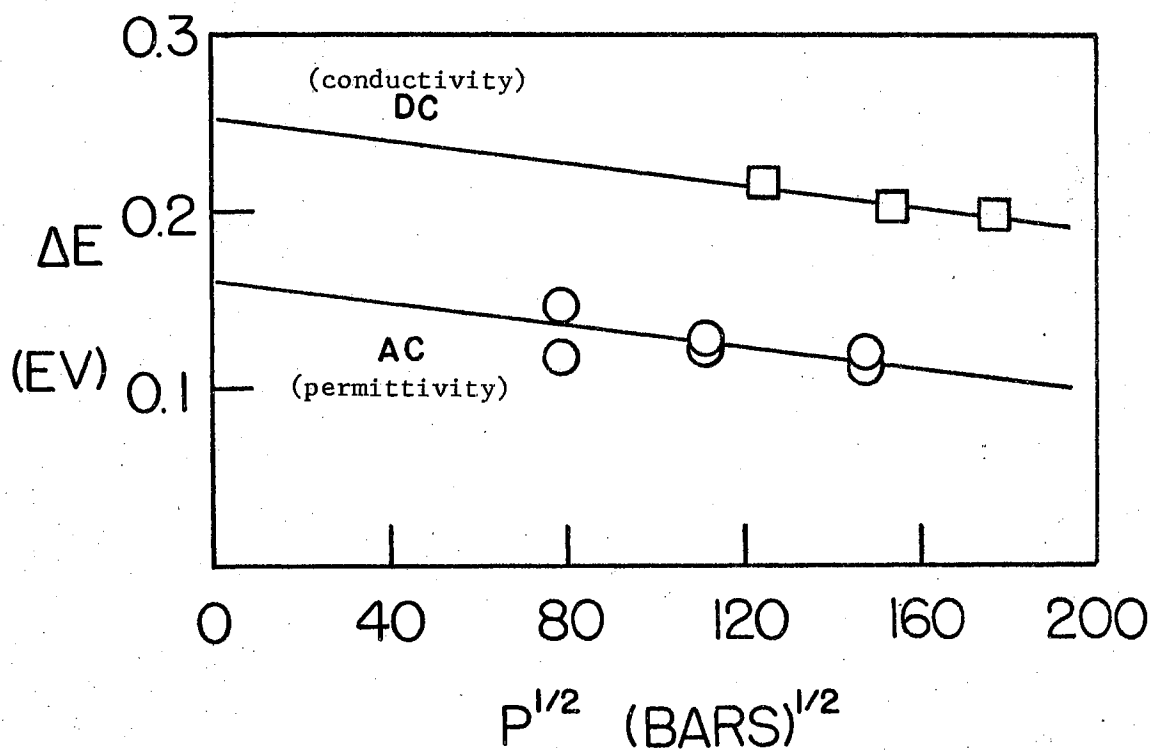
Figure 7. The Energy Interval, ΔE, as a Function of the Square Root of Pressure for the 9-Thioxanthane-PMA Polymer

TABLE V

THE TOTAL CONDUCTIVITY PRESSURE COEFFICIENT

	$b_T^{\sigma} \times 10^6$ eV(bars)$^{\frac{1}{2}}$ $^{\circ}$K				
Sample	D.C.	100Hz	1kHz	10kHz	100kHz
Acridone-PMA	1.82	2.73	2.67	2.59	2.28
Acridone-MTA	1.51	2.97	2.86	2.68	1.80
Thianthrene-PMA	2.22	2.37	2.37	2.37	2.37
Thianthrene-MTA	2.31	3.35	3.35	3.35	3.35
Anthrone-MTA	1.41	2.71	2.60	2.40	1.65
9-Thioxanthane-PMA	1.82	2.06	2.06	2.03	1.98
Carbazole-MTA	1.26	1.96	1.94	1.87	1.82

TABLE VI

THE TOTAL PERMITTIVITY PRESSURE COEFFICIENT

	$b_T^{\epsilon} \times 10^6$ eV/(bars)$^{\frac{1}{2}}$ $^{\circ}$K			
Sample	100Hz	1kHz	10kHz	100kHz
Acridone-PMA	--	2.34	1.65	0.90
Acridone-MTA	1.80	1.45	1.32	0.74
Thianthrene-PMA	--	2.37	2.39	2.36
Thianthrene-MTA	2.40	2.40	2.40	2.40
Anthrone-MTA	2.20	1.64	1.32	0.86
9-Thioxanthane-PMA	1.23	1.23	1.21	--
Carbazole-MTA	1.14	1.21	1.07	1.02

same decrease with frequency is observed, but the values are lower. The ratio of the total pressure coefficients is shown in Table VII. In general, the ratios range from 1 to 2 and increase with frequency. This suggests that for an increment increase of pressure the electron transfer process between molecules is increased, but the conduction increases even more rapidly, as would be expected for hopping conduction.

TABLE VII.

THE RATIO OF CONDUCTIVITY TO PERMITTIVITY
PRESSURE COEFFICIENTS

| Sample | $(b_T^{\sigma} / b_T^{\epsilon})$ | | | |
| | Frequency | | | |
	100Hz	1kHz	10kHz	100kHz
Acridone-PMA	--	1.14	1.57	2.53
Acridone-MTA	1.65	1.97	2.03	2.43
Thianthrene-PMA	--	1.00	0.99	1.00
Thianthrene-MTA	1.40	1.40	1.40	1.40
Anthrone-MTA	1.23	1.59	1.82	1.92
9-Thioxanthane-PMA	1.67	1.67	1.68	--
Carbazole-MTA	1.70	1.60	1.75	1.78

Other conjugated polymer systems have also been investigated (163). The results are similar and suggest mechanisms similar to those proposed for the PAQR samples.

Kho and Pohl (140) have extensively studied the pressure effects as a function of chemical structure. They have shown that a decrease in the pressure coefficient occurs when the number of fused rings is increased for PAQR homopolymers. This supports the original assumptions that the effect of pressure on the "area of contact" or orbital overlap depends on the starting overlap. As the number of fused rings increases, the overlap increases. For the same reason the energy interval decreases when the number of fused rings is increased. The increase in pressure coefficient with increasing energy interval has also been observed for the polymer samples investigated here. The results are shown in Figure 8.

The results can then be generalized:

$$(b_E^{\sigma})_{AC} = (b_E^{\sigma})_{DC} = (b_E^{\sigma})_{AC} \tag{8}$$

$$(b_E) \neq f(\omega) \tag{9}$$

$$(b_T^{\sigma})_{DC} < (b_T^{\sigma})_{AC} \tag{10}$$

$$(b_T^{\epsilon})_{AC} < (b_T^{\sigma})_{AC} \tag{11}$$

$$(\Delta E)_{AC} < (\Delta E)_{DC} \tag{12}$$

$$(\Delta E_{\sigma})_{AC} = (\Delta E_{\epsilon})_{AC} \; . \tag{13}$$
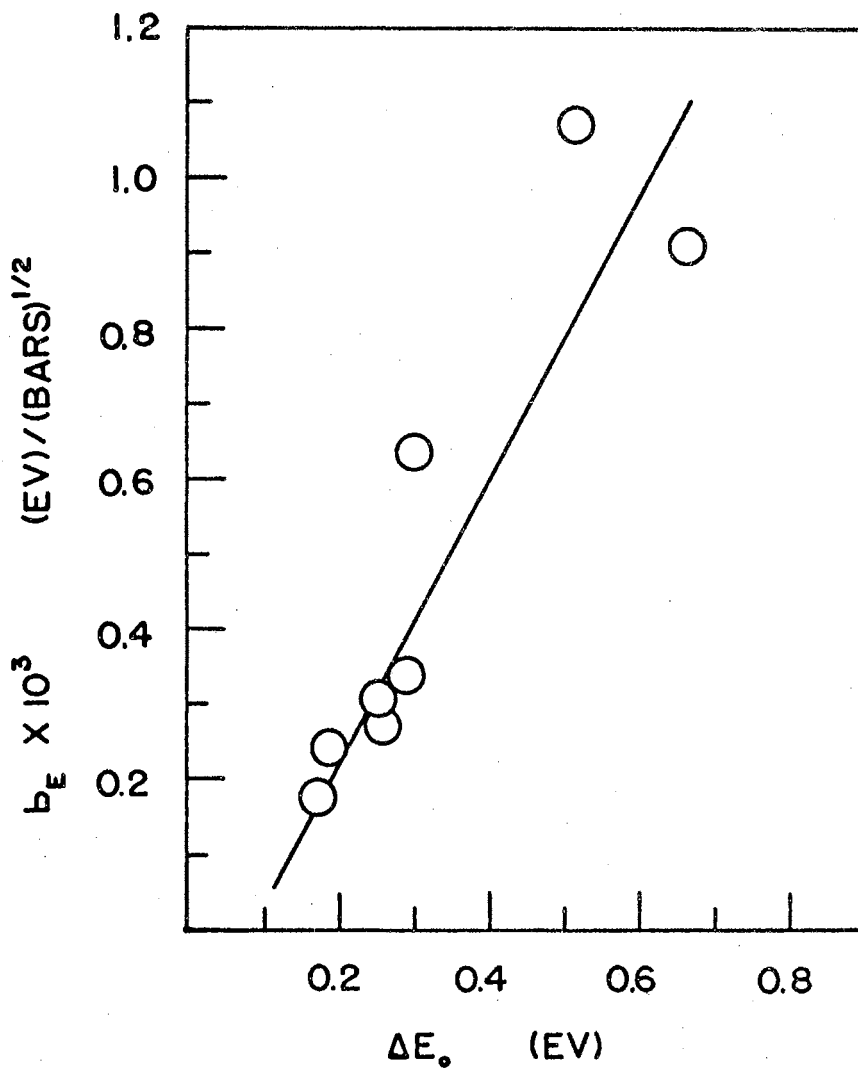
Figure 8. The Value of b_E as a Function of the Energy Interval at Zero Pressure ΔE_o for Several PAQR Polymers

Effects of A. C. Field Intensity

The effect of an applied a. c. field on polymers exhibiting hyper-electronic polarization was observed by Rosen and Pohl (1). They reported a decrease in the permittivity as the field intensity was increased. The greatest decrease occurred at lower frequencies. Hartman (3) suggested by means of a simple model that the decrease of the permittivity was inversely proportional to the electric field applied across the sample, although the data reported suggested the actual decrease was proportional to $\mathcal{E}^{-\frac{1}{2}}$.

The measurement of the a. c. conductivity and permittivity has been described in Chapter II. For most samples the field intensities ranged from 1 to 1000 volts/cm. Typical results are shown in Figure 9. The permittivity is plotted as a function of the field intensity on a log-log scale. For these samples the frequency was 1000 Hz and the pressure approximately 10 kilobars. The permittivity has its maximum value at low field intensities, 1-10 volts/cm. From this model this would be expected, since the charge is displaced to the extremities of the molecules by a very small field. The observed polarization is a function of this displacement. The relative permittivity ϵ_r is defined by the relationship

$$(\epsilon_r - 1) = \frac{\vec{P}}{\epsilon_o \vec{\mathcal{E}}} \quad . \tag{14}$$

For discussions of hyperelectronic polarization the value of ϵ_r is much greater than 1, and equation (14) can be approximated by

$$\epsilon_r \cong \frac{\vec{P}}{\epsilon_o \vec{\mathcal{E}}} \tag{15}$$
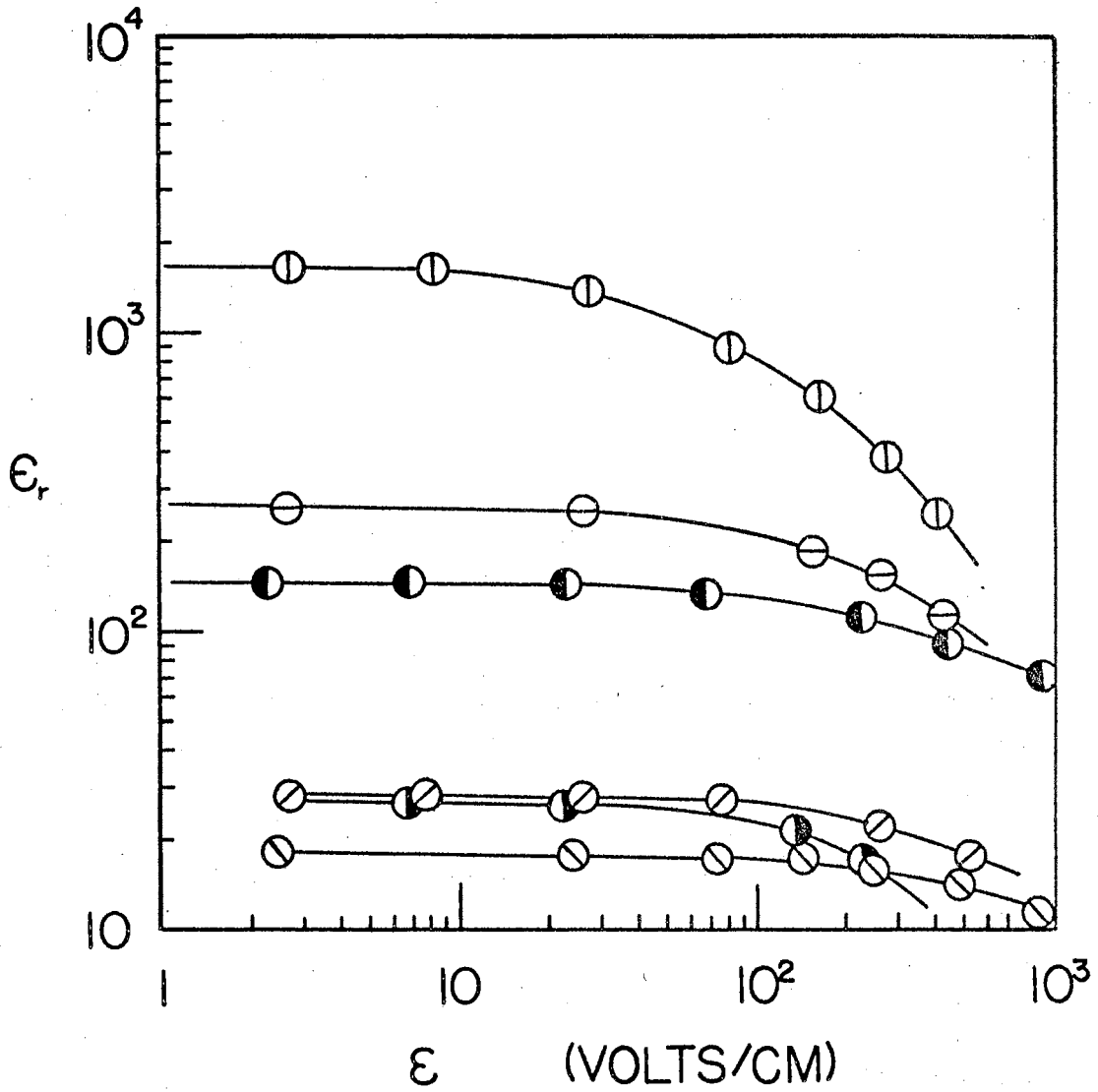
Figure 9. The Permittivity ϵ_r at 1000Hz as a Function of Field
Intensity $\mathcal{E}$ for Six PAQR Polymers

where $\vec{P}$ is the polarization vector and ϵ_o is the permittivity of free space. The polarization vector is defined as the dipole moment per unit volume,

$$\vec{P} = N\vec{\mu}$$

(16)

where $\vec{\mu}$ is the average dipole moment and N is the number of dipoles.

The data indicate that for very low field intensities, the polarization is directly proportional to the field intensity, and thus ϵ_r is constant. But for higher fields the polarization does not continue to increase at the same rate as the field intensity and the permittivity decreases. This may be due to a decrease in the number of interacting dipoles or a limitation on the average dipole moment or a combination of both. Figure 10 shows the results for the phenothiazene-PMA sample when the polarization is plotted as a function of the field intensity. The polarization vector was determined from equation (15).

In order to obtain a quantitative empirical expression for the field dependency of the permittivity, the data were plotted in a different form, which results in a straight line on a log-log scale with a slope equal to unity. This can be done by plotting $\ln(\epsilon_r'/\epsilon_r - 1)$ as a function of field intensity. The quantity ϵ_r' is the value of ϵ_r when the field intensity approaches zero. Then the relation becomes,

$$\ln\left(\frac{\epsilon_r'}{\epsilon_r} - 1\right) = \ln\mathcal{E} - \ln\mathcal{E}_{\frac{1}{2}}$$

(17)

where $\mathcal{E}_{\frac{1}{2}}$ is the value of $\mathcal{E}$ when ϵ_r is equal to $\frac{1}{2}\epsilon_r'$. Then

$$\left(\frac{\epsilon_r'}{\epsilon_r} - 1\right) = \frac{\mathcal{E}}{\mathcal{E}_{\frac{1}{2}}},$$

(18)

and solving for ϵ_r ,
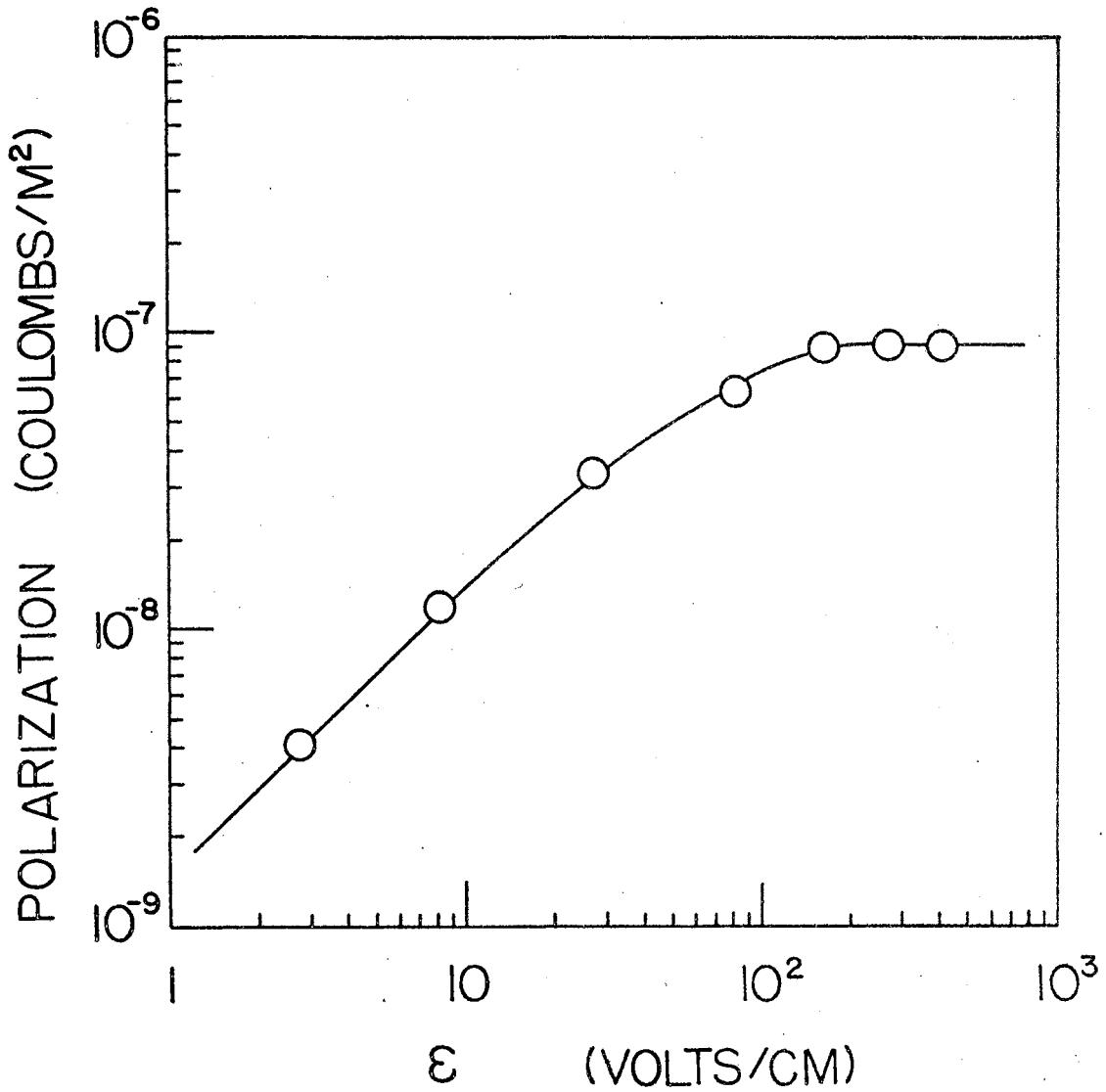
Figure 10. The Polarization $\vec{P}$ as a Function of Field Intensity $\vec{\mathcal{E}}$ for the Phenothiazene-PMA Polymer at a Frequency of 1000 Hz

$$\epsilon_r = \frac{\epsilon'_r \mathcal{E}_{\frac{1}{2}}}{(\mathcal{E} + \mathcal{E}_{\frac{1}{2}})} \quad . \tag{19}$$

Figure 11 shows the results for the phenothiazene-PMA polymer plotted in this manner. The data was obtained at a pressure of 3.2 kbars and a temperature of 297°K. The results for three frequencies lie essentially on the same line, indicating a constant value for $\mathcal{E}_{\frac{1}{2}}$. This implies that the rate of decrease in the permittivity is independent of frequency and the permittivity attains half the zero field value at the same field intensity.

The value of $\mathcal{E}_{\frac{1}{2}}$ is changed by pressure as shown in Figure 12. Here the results are shown for the 9-thioxanthane-PMA sample at three intermediate pressures at a constant frequency of 1000 Hz. The values of ϵ'_r, $\mathcal{E}_{\frac{1}{2}}$ and the product of $\epsilon'_r \mathcal{E}_{\frac{1}{2}}$ are shown in Table VIII. Although ϵ'_r increases with pressure, $\mathcal{E}_{\frac{1}{2}}$ decreases, and the product remains constant.

TABLE VIII

THE PERMITTIVITY FIELD EFFECT RESULTS

Pressure (kbars)	ϵ'_r	$\mathcal{E}_{\frac{1}{2}}$ (v/cm)	$\epsilon'_r \mathcal{E}_{\frac{1}{2}}$ (v/cm)
9.4	104	2370	2.46×10^5
15.7	152	1650	2.51×10^5
23.6	235	1080	2.54×10^5

The value of ϵ'_r would be expected to be a function of frequency
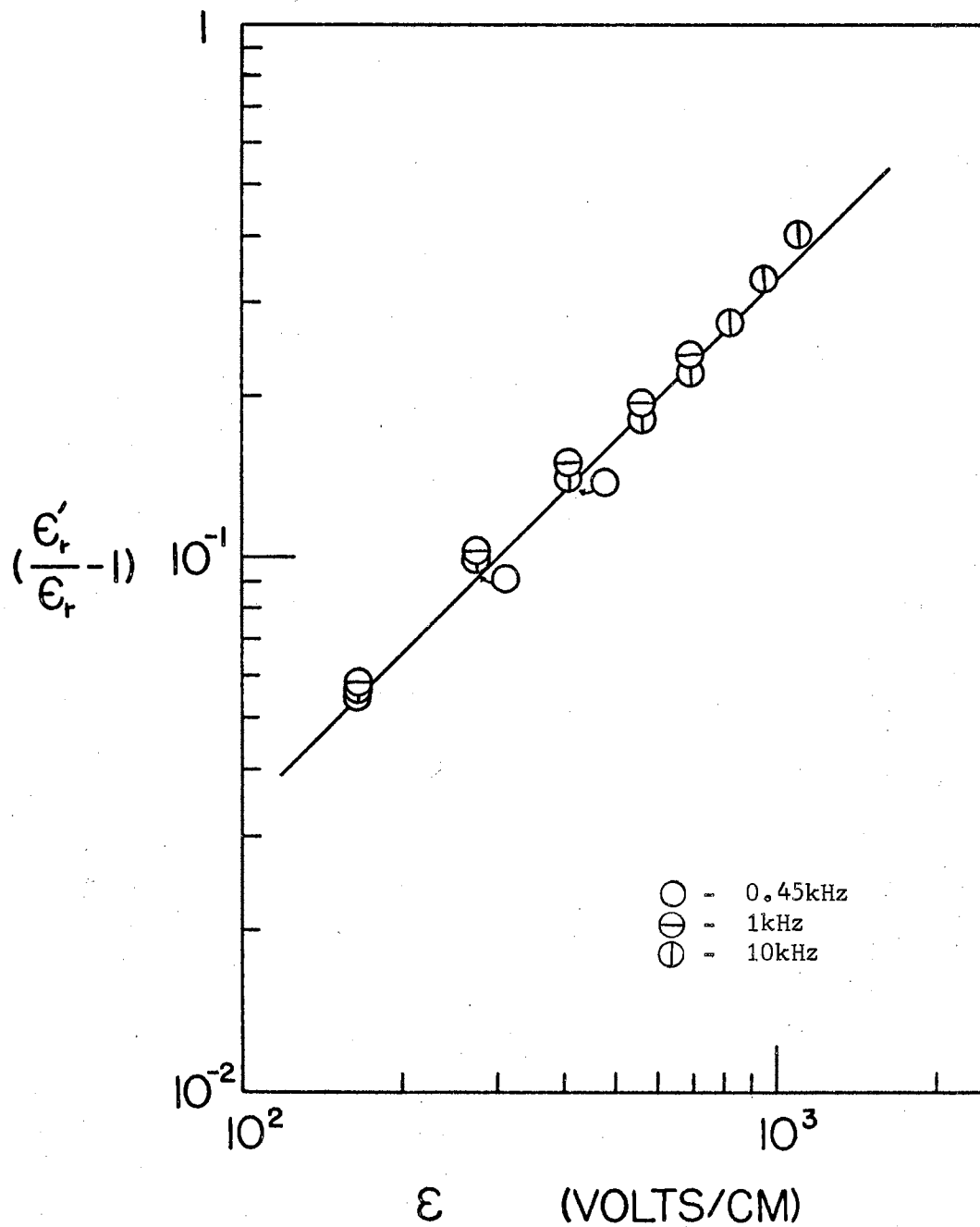
Figure 11. The Value of (ϵ_r' /ϵ_r - 1) as a Function of Field In-
tensity $\mathcal{E}$ for the Phenothiazene-PMA Polymer at a
Temperature of 297°K and Pressure of 3.2 Kilobars
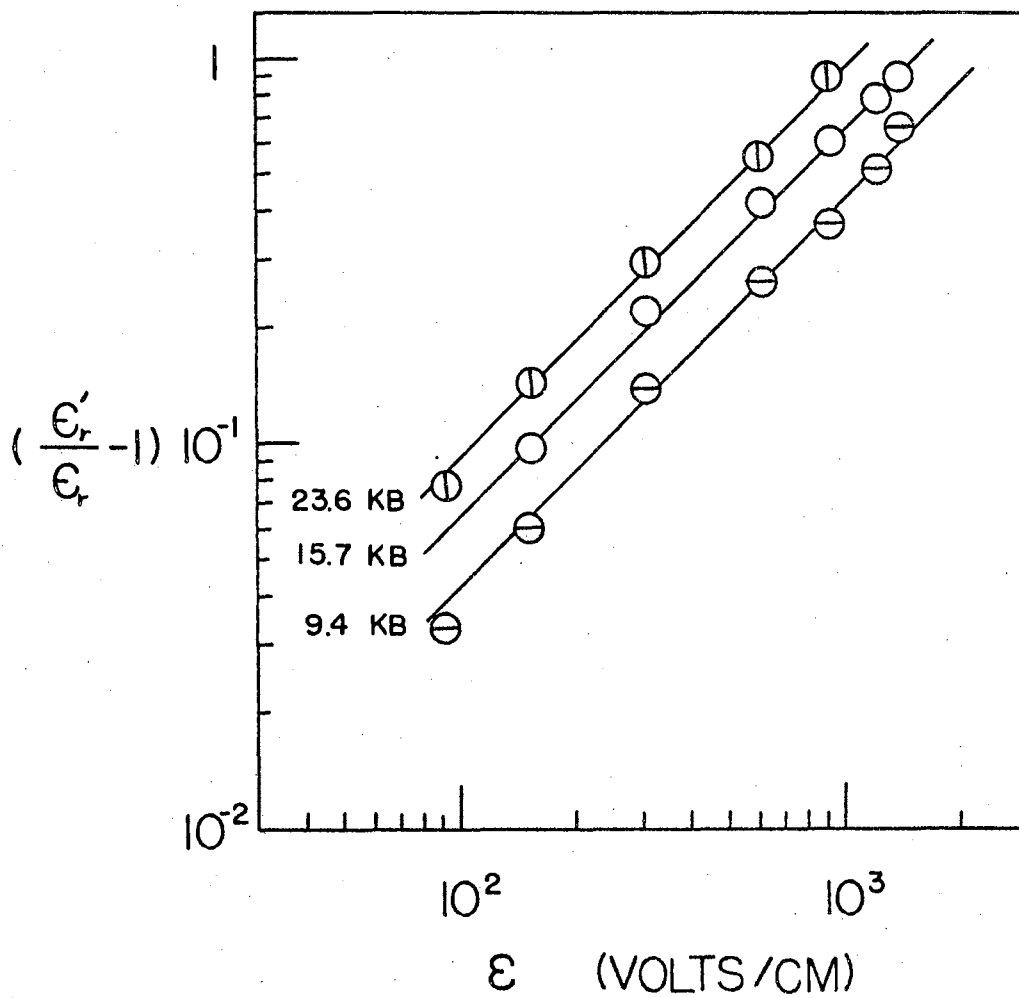
Figure 12. The Value of $(\epsilon'_r/\epsilon_r - 1)$ as a Function of Field
Intensity ϵ for the 9-Thioxanthane-PMA Polymer
at a Frequency of 1000Hz and Temperature of $297°K$

and pressure in the same manner as ϵ_r since it is equal to one-half the maximum value of ϵ_r. From these low frequency results, which are attributed entirely to hyperelectronic polarization, the value of $\epsilon_{\frac{1}{2}}$ is independent of frequency but inversely dependent upon external pressure.

From equation (19) it can be seen that as the value of $\epsilon_{\frac{1}{2}}$ decreases the field effect is increased. For very high values of $\epsilon_{\frac{1}{2}}$, i. e. $\epsilon_{\frac{1}{2}} \gg \epsilon$, the field effect is negligible. This would occur at low pressure. Thus $\epsilon_{\frac{1}{2}}$ may be a reflection of the number of interacting dipoles or macropoles contributing to hyperelectronic polarization.

Typical results for the a. c. conductivity are shown in Figure 13. The data are plotted in a form developed from equation (5) in Chapter II. The results agree with the d. c. conductivity field effect predicted by Rosen and Pohl (1). It should be noted here that the relationship is independent of pressure for a large pressure range.

It was suggested by M. Knotek (164) that an expression for the potential as seen by the polarizing charge could be obtained from equation (19). For small dipole-dipole interaction, the electron can be placed in a potential well and the field response used to determine the shape of the well. The electron will move under the influence of the external field according to the expression

$$\epsilon = -\partial \phi / \partial x \qquad (20)$$

where ∂x is the distance moved in the potential $\partial \phi$. The dipole moment is then

$$ex = \propto \epsilon \qquad (21)$$

where e is the electronic charge and $\propto$ is the polarizability, defined as

$$\propto = \epsilon_r \epsilon_o / n \qquad (22)$$
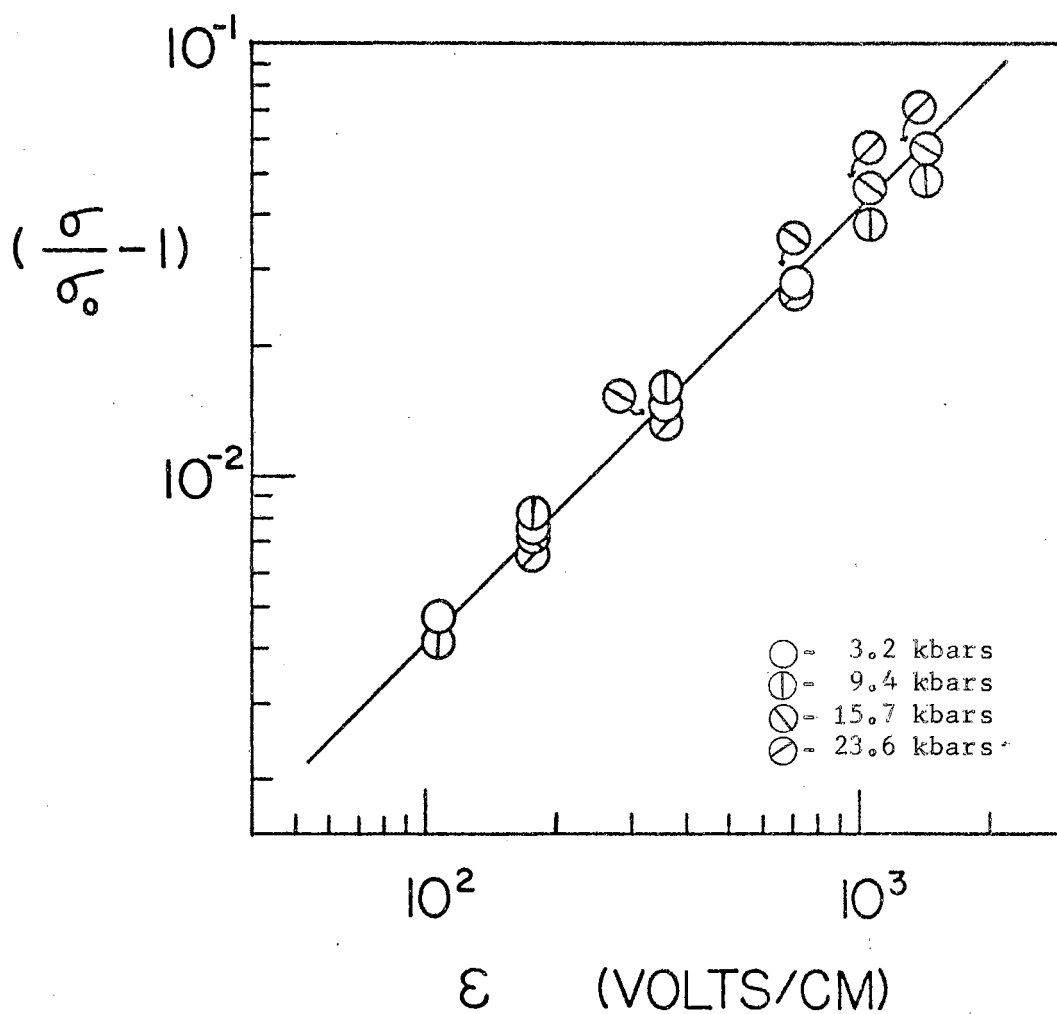
Figure 13. The Value of $(\sigma/\sigma_o - 1)$ as a Function of Field Intensity $\mathcal{E}$ for the Anthracene-PMA Polymer at a Frequency of 1000Hz and Temperature of $297^{\circ}K$

where n is the number of monopoles. Including the field effect from

equation (19),

$$\propto \; = \; \frac{\epsilon'_r \epsilon_o \mathcal{E}_{\frac{1}{2}}}{n \; (\mathcal{E} + \mathcal{E}_{\frac{1}{2}})} \; . \qquad (23)$$

Then substituting into equation (21),

$$e \, x \; = \; \frac{\epsilon'_r \epsilon_o \mathcal{E}_{\frac{1}{2}}}{n \; (\mathcal{E} + \mathcal{E}_{\frac{1}{2}})} \; . \qquad (24)$$

Then solving for the field intensity,

$$\mathcal{E} \; = \; \frac{x \mathcal{E}_{\frac{1}{2}}}{x - \dfrac{\epsilon'_r \epsilon_o \mathcal{E}_{\frac{1}{2}}}{n \, e}} \; = \; - \frac{\partial \phi}{\partial x} \; , \qquad (25)$$

and then integrating equation (25),

$$- \phi(x) \; = \; \mathcal{E}_{\frac{1}{2}} x + \left(\frac{\epsilon'_r \epsilon_o \mathcal{E}^2_{\frac{1}{2}}}{n \, e} \right) \ln \left[1 - \frac{n \, e \, x}{\epsilon'_r \epsilon_o \mathcal{E}_{\frac{1}{2}}} \right] \; . \qquad (26)$$

If one lets

$$L_o \; = \; \frac{\epsilon'_r \epsilon_o \mathcal{E}_{\frac{1}{2}}}{n \, e} \; , \qquad (27)$$

then equation (26) becomes

$$- \phi(x) \; = \; \mathcal{E}_{\frac{1}{2}} x + \mathcal{E}_{\frac{1}{2}} L_o \ln \left(1 - \frac{x}{L_o} \right) \; . \qquad (28)$$

Then as x approaches the value of L_o , the potential approaches in-

finity very rapidly. When x is small compared to L_o , the first

term, which is linear with x , is predominant. Thus the field re-

sponse suggests a potential well or almost square well box. The quan-

tity $L_o n$ can now be evaluated for the samples measured. If the value

of n, the number of dipoles per unit volume, can be determined, then

the molecular length can be determined.

Table IX gives the values of $\epsilon'_r \mathcal{E}_{\frac{1}{2}}$ for six samples at four lower

frequencies. The units of $\epsilon_r' \mathcal{E}_{\frac{1}{2}}$ are volts/cm. The frequency dependency is small for lower frequencies.

TABLE IX

THE LOW-FREQUENCY VALUES OF $\epsilon_r' \mathcal{E}_{\frac{1}{2}}$ (V/CM)

| Sample | (Frequency, Hz) | | | |
	45	100	1000	10,000
Carbazole-PMA	--	--	3.04×10^4	7.92×10^4
Acridone-PMA	1.18×10^5	1.35×10^5	6.10×10^4	--
Dibenzofuran-PMA	--	3.49×10^4	2.52×10^4	1.42×10^4
Phenothiazene-PMA	--	--	9.37×10^3	4.90×10^4
Phenoxathiin-PMA	7.45×10^4	8.58×10^4	1.02×10^5	--
Carbazole-MTA	--	3.15×10^6	1.50×10^6	1.44×10^6

If the molecules are assumed to be rod-like, a rough calculation of the thickness can be made. If one lets A be the cross-sectional area of the molecules, then

$$AL_o \;=\; 1 / n_o \tag{29}$$

where n_o is the number of molecules per unit volume. Then substituting for L_o,

$$\frac{A \epsilon_r' \epsilon_o \mathcal{E}_{\frac{1}{2}}}{n\,e} \;=\; \frac{1}{n_o} \tag{30}$$

where n is the number of molecules in the activated state taking part in producing the hyperelectronic polarization. The ratio of n / n_o is related to the activation energy by the expression

$$\frac{n}{n_o} = e^{-\frac{E_a}{kT}}$$

(31)

where E_a is the thermal activation energy of carriers and monopoles

and n_o is the number activated when $T \rightarrow \infty$.

Substituting equation (31) into equation (30), and solving for A,

$$A = \frac{e}{\epsilon_o \epsilon_r' \mathcal{E}_{\frac{1}{2}}} \exp \left[-\frac{E_a}{kT} \right].$$

(32)

A sample calculation for the carbazole-MTA polymer was as follows:

E_a = 0.243 eV at 10 kilobars

$\epsilon_r' \mathcal{E}_{\frac{1}{2}}$ = 1.50 x 10^7 volts/meter at 10 kilobars

e = 1.602 x 10^{-19} coulomb

ϵ_o = 8.8542 x 10^{-12} farad/meter

k = 0.8617 x 10^4 eV/$^\circ$K

T = 297°K .

Substituting these values into equation (32),

A = 9.033 x 10^{-20} m^2

= 9.033 $\overset{o}{A}^2$.

Then if $A = \pi r^2$, $r = 1.70$ $\overset{o}{A}$ and the diameter of the rod-like molecule

is 3.40 $\overset{o}{A}$. Although this is a rough approximation, the resulting value

agrees well with x-ray determinations of 3.4 $\overset{o}{A}$.

Frequency Effects

The frequency response data for the permittivity and conductivity

were obtained by the technique described in Chapter III. A very

pronounced frequency response of the permittivity is shown in Figure 14. The attenuation of the permittivity with increasing frequency is more rapid for the higher temperature. All of the samples measured showed a permittivity frequency response approximating the relation,

$$\epsilon_r = B\,\omega^{-p} \tag{33}$$

where B and p are constants. The relation was quite good for the lower frequencies, i.e. less than 10kHz, but deviations occurred at higher frequencies, possibly due to measurement error.

The conductivity increased at high frequencies. This effect has been observed by Hartman (3) for similar samples, and was attributed to hopping conduction. The impurity-band conduction model, developed by Mott (165), has been recently applied to highly disordered or amorphous structures by Fritzsche (166). The band model for amorphous structures requires overlapping conduction and valance band tails of localized states and sharp mobility edges at the conduction and valance band energy levels. The mobility gap, rather than a forbidden energy gap, gives rise to the well defined thermal activation energy or energy interval of the electrical conductivity.

The model developed by Pollak and Geballe (167) consists of an electron confined to a pair of acceptors. A d. c. electric field polarizes the pair, permitting time for transition. The current is the derivative of the polarization with time. If an a. c. electric field is applied with a frequency greater than the transition rate, the resulting polarization will lag behind the applied field. Thus, part of the polarization will be out of phase with the applied field and will be measured as a dielectric loss. As the frequency is increased, the out-of-phase part of the polarization, or the a. c. conductivity, will
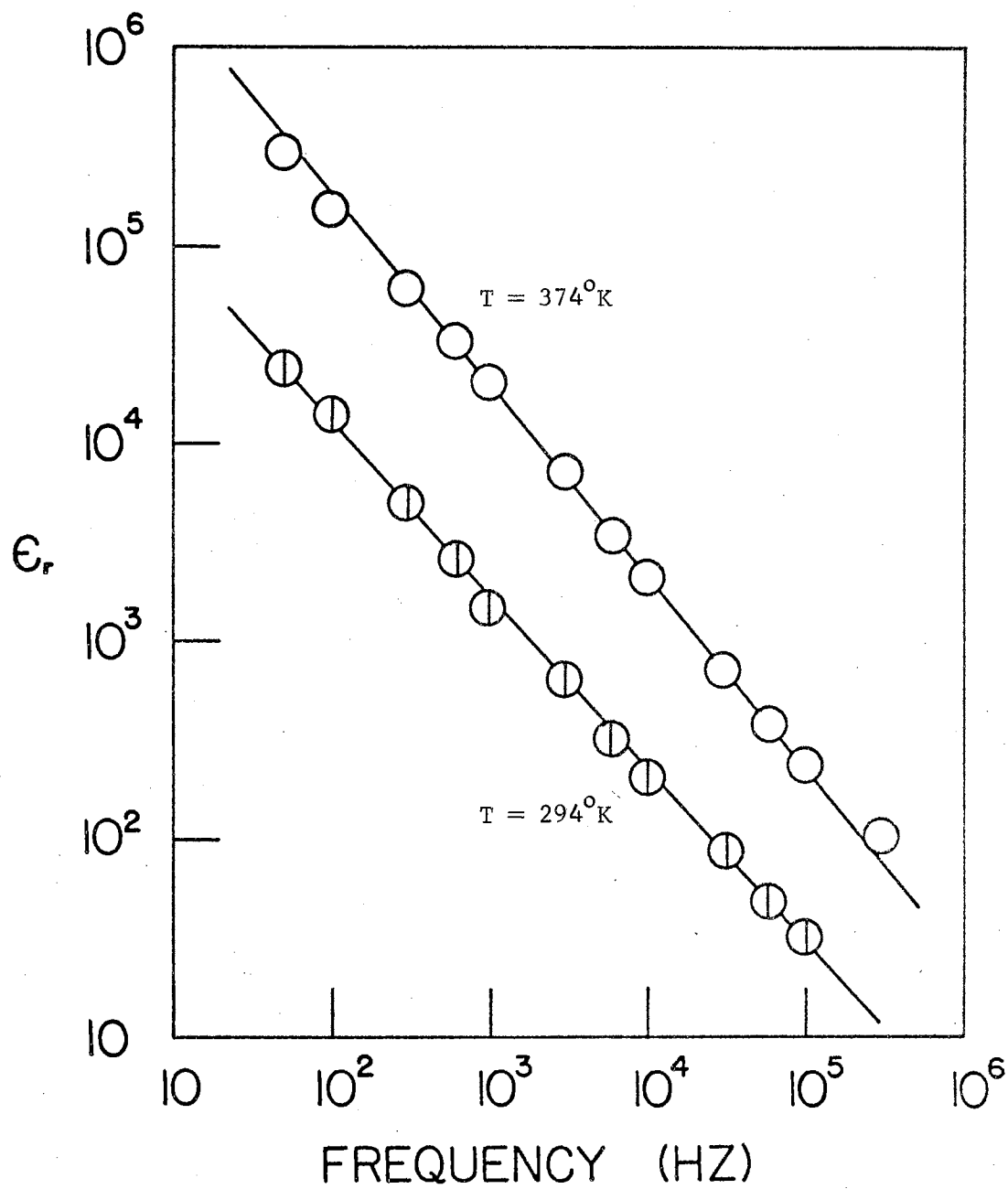
Figure 14. The Relative Permittivity as a Function of Frequency for
the Carbazole-MTA Polymer at 6.3 Kilobars

increase. It is assumed that the electron is localized on a pair of acceptors (168). The model predicts a square-law frequency dependence of the a. c. conductivity at frequencies high compared to the transition rate, i.e. $\sigma_{AC} = k\omega^2$.

The a. c. conductivity can be presented as a complex quantity in a similar manner as the permittivity. The complex permittivity is given by

$$\epsilon^* = \epsilon' - i\epsilon'' \tag{34}$$

where ϵ' is the real part and ϵ'' is the imaginary part. The complex conductivity is given by

$$\sigma^* = \sigma' - i\sigma'' \tag{35}$$

where σ' is the real part and σ'' is the imaginary part. The real part of the conductivity is related to the imaginary part of the permittivity, using the notation of von Hippel (2), by the relation

$$\epsilon'' = \frac{\sigma'}{\omega} \tag{36}$$

and analagously,

$$\sigma'' = \omega\epsilon' \tag{37}$$

where ω is the angular frequency.

The conductivity referred to in this discussion is the a. c. conductivity. Thus the measured conductivity σ is given by

$$\sigma = \sigma_{DC} + \sigma_{AC} \tag{38}$$

where $\sigma_{AC} = \sigma'$. The relative permittivity ϵ_r is then related to the imaginary conductivity by the expression

$$\sigma'' = \epsilon_r \epsilon_o \omega . \tag{39}$$

The frequency dependence can be related by the equation suggested by Pollak and Geballe (167),

$$\sigma_{AC} = \sigma - \sigma_{DC} = A\omega^s \tag{40}$$

where A is complex and s has values between 0.4 and 0.9 for samples measured in this investigation. Then,

$$\sigma' = \text{Re}(A)\omega^s \tag{41}$$

and

$$\sigma'' = \epsilon_r\epsilon_o\omega = \text{Im}(A)\omega^s . \tag{42}$$

Equation (42) can be related to the equation (33) if

$$B = \epsilon_o\text{Im}(A)$$

$$\tag{43}$$

$$p = 1 - s .$$

Figures 15-21 show the results for seven polymers. The real and imaginary parts of the a. c. conductivity are plotted as a function of frequency for high and low pressures. The values of s are approximately the same for the different pressures. In general, the a. c. conductivities are determined from the high frequency results, while the permittivity values are determined from low frequency results. Although the values of s for the real and imaginary parts of the conductivity are approximated equal, they were not determined for the same frequency range. If equation (40) is valid for a wide frequency range, the Kramers-Kronig relation (168) can be used to relate the real and imaginary parts,

$$\frac{\sigma''}{\sigma'} = \tan\left(\tfrac{1}{2}\pi s\right) . \tag{44}$$
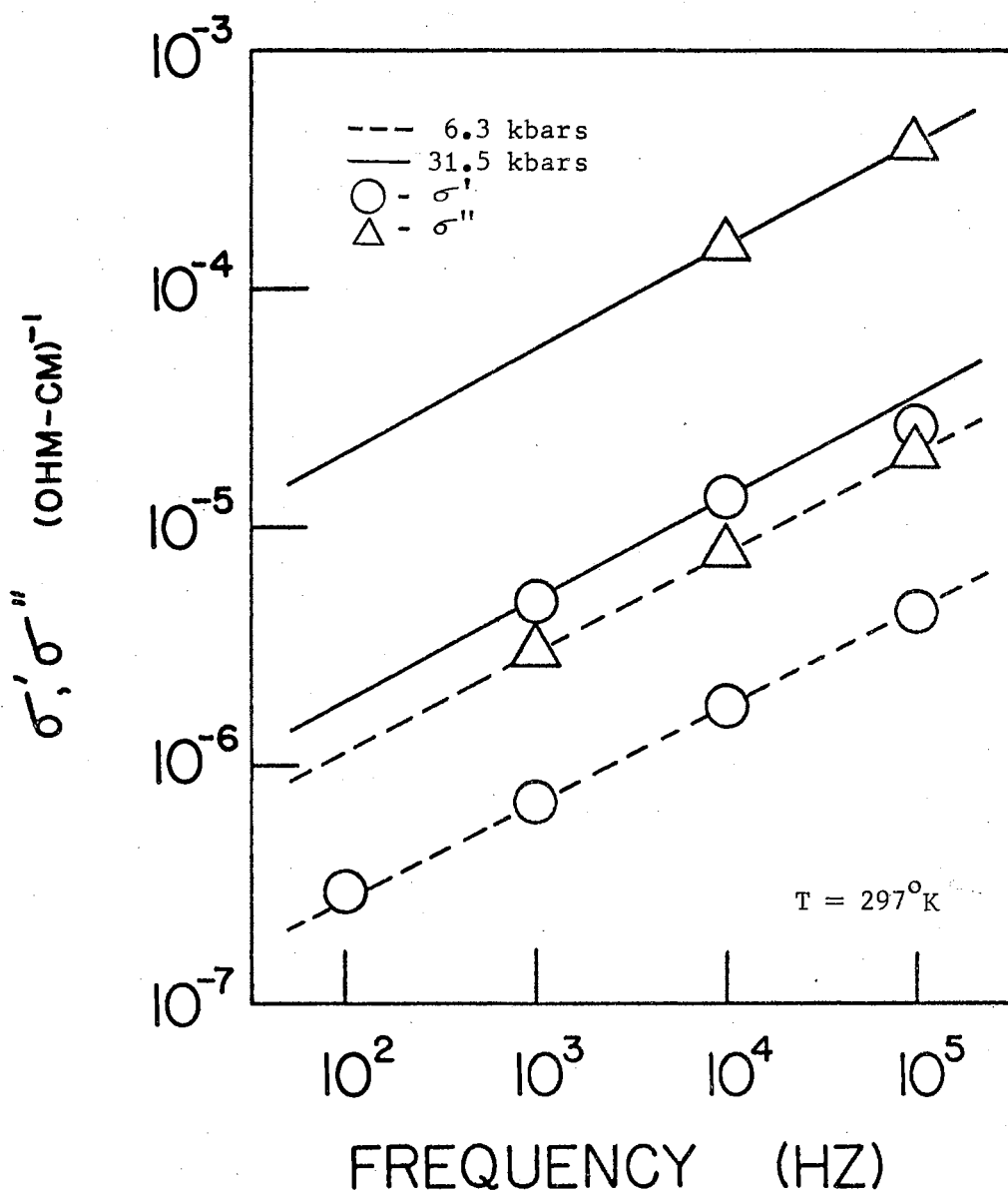
Figure 15. The Real σ' and Imaginary σ'' Parts of the Complex Conductivity for the Thianthrene-PMA Polymer as a Function of Frequency
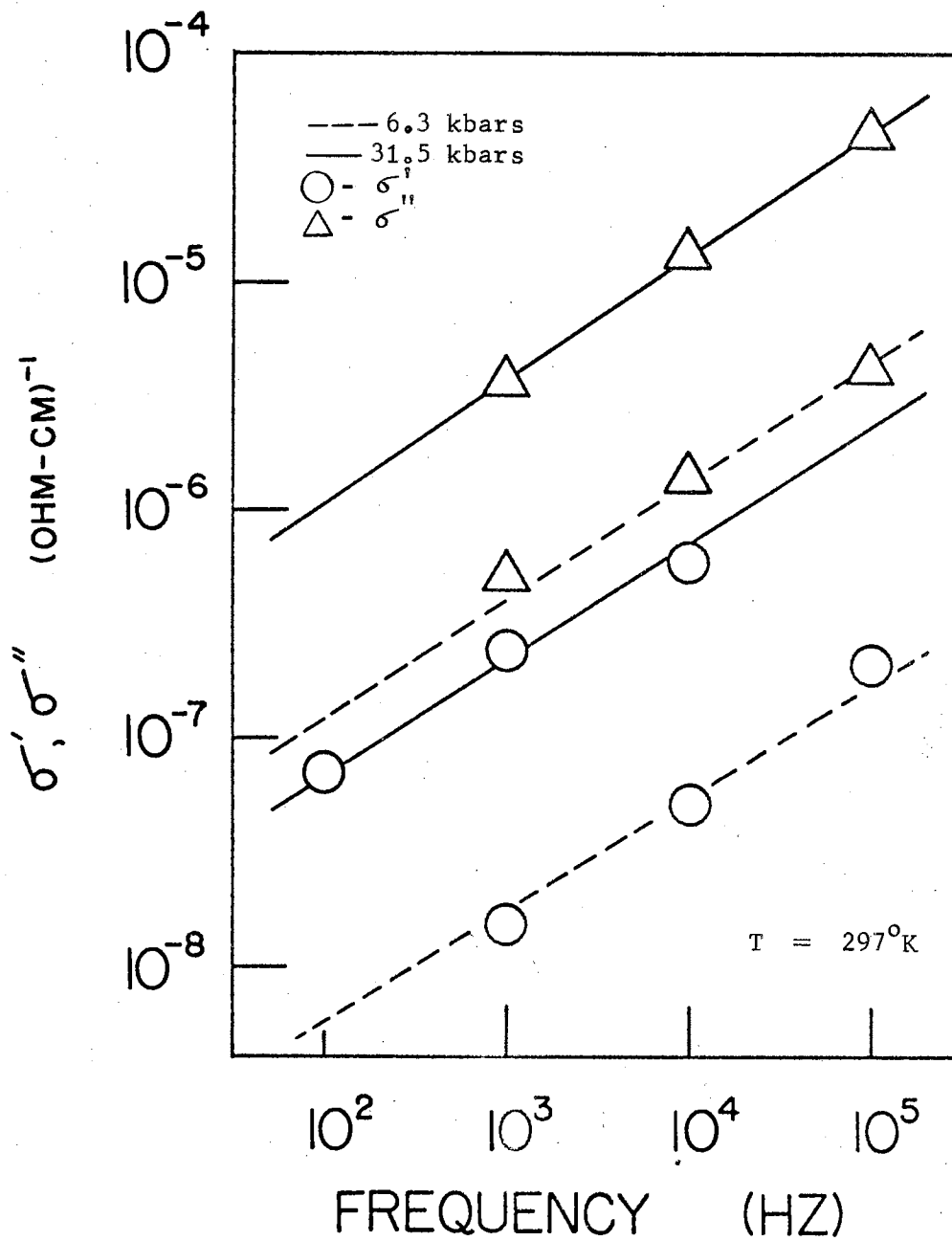
Figure 16. The Real σ' and Imaginary σ'' Parts of the Complex Conductivity for the Thianthrene-MTA Polymer as a Function of Frequency
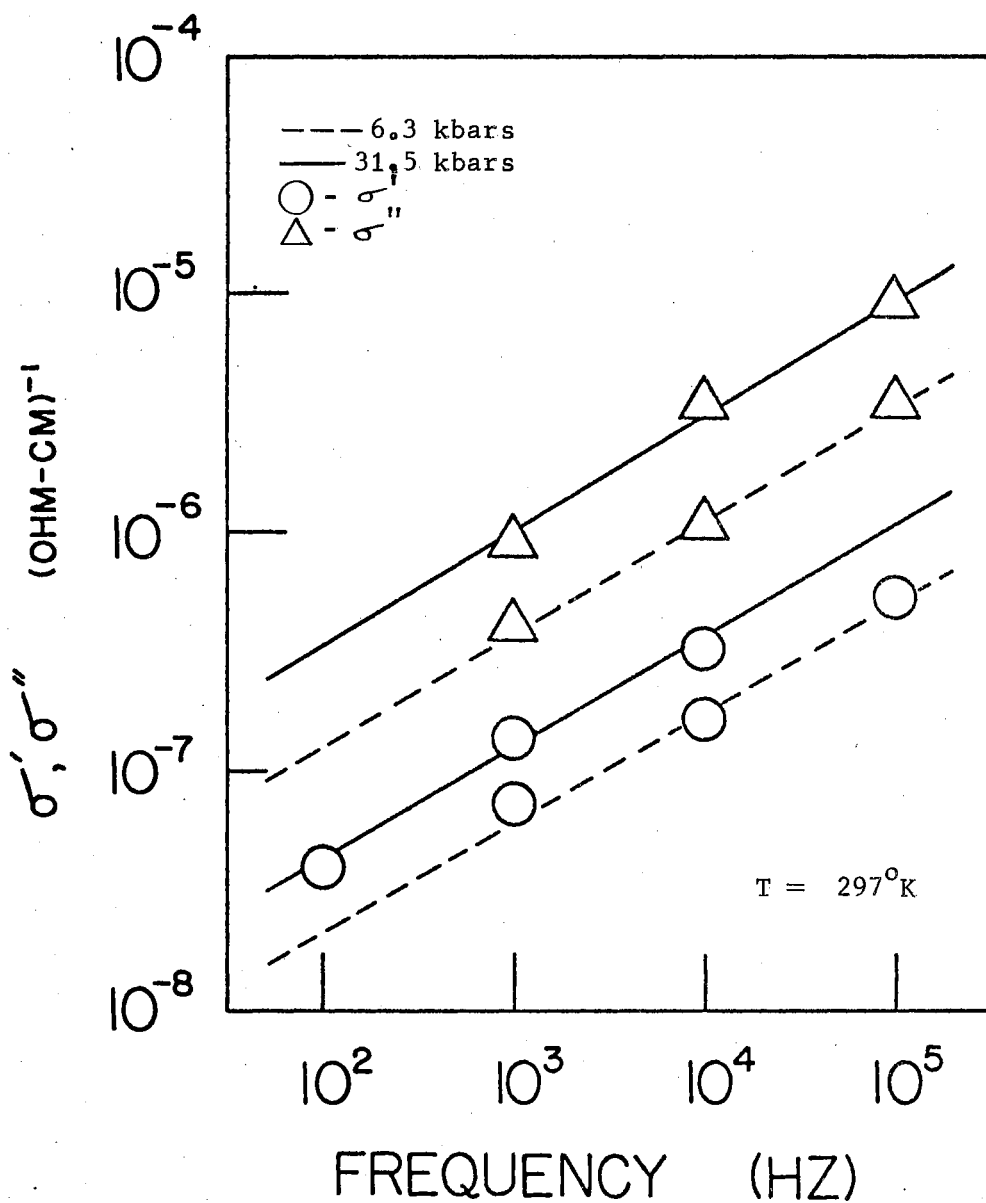
Figure 17. The Real σ' and Imaginary σ'' Parts of the Complex Conductivity for the Dibenzofuran-PMA Polymer as a Function of Frequency
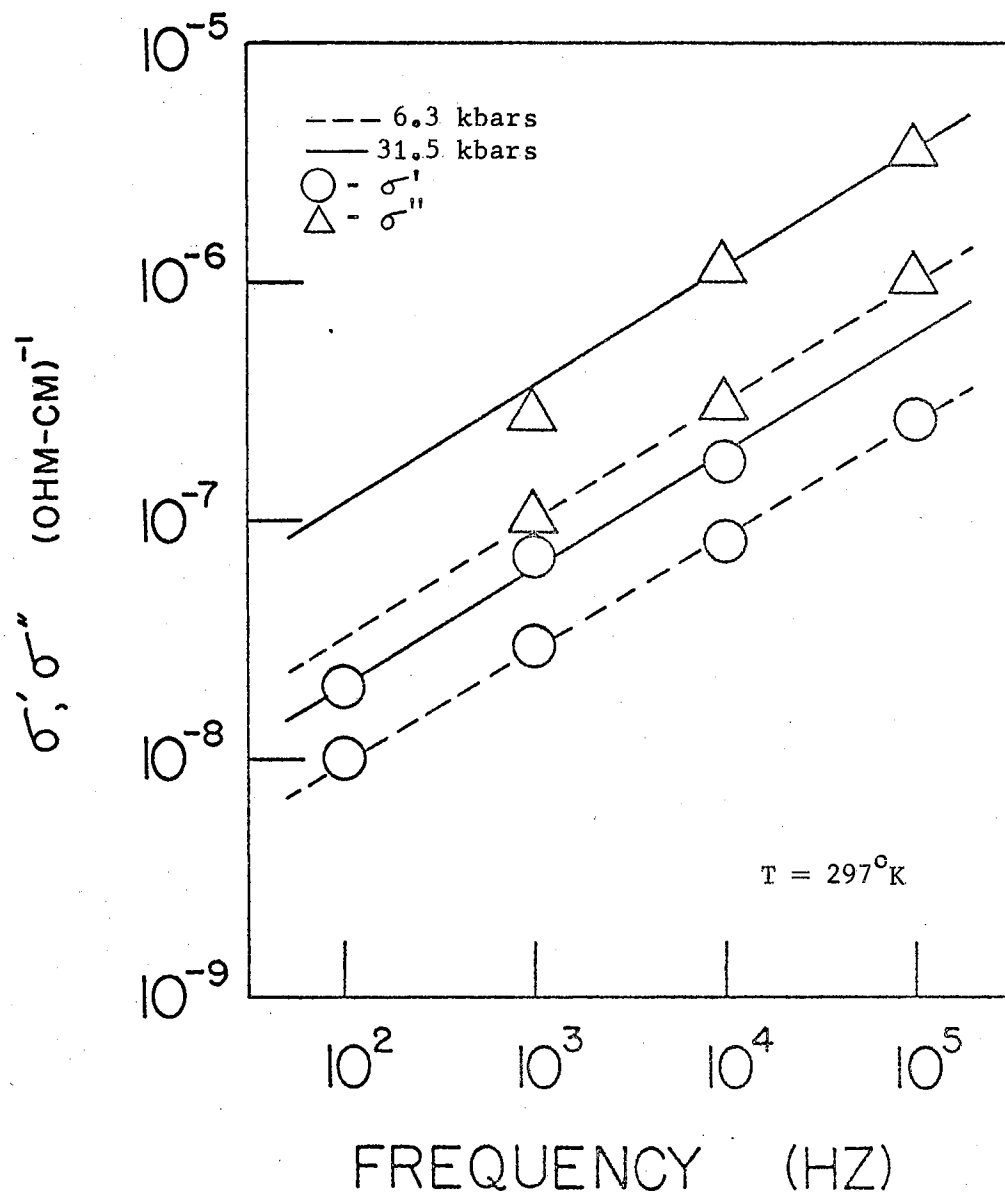
Figure 18. The Real σ' and Imaginary σ'' Parts of the Complex Conductivity for the Xanthone-PMA Polymer as a Function of Frequency
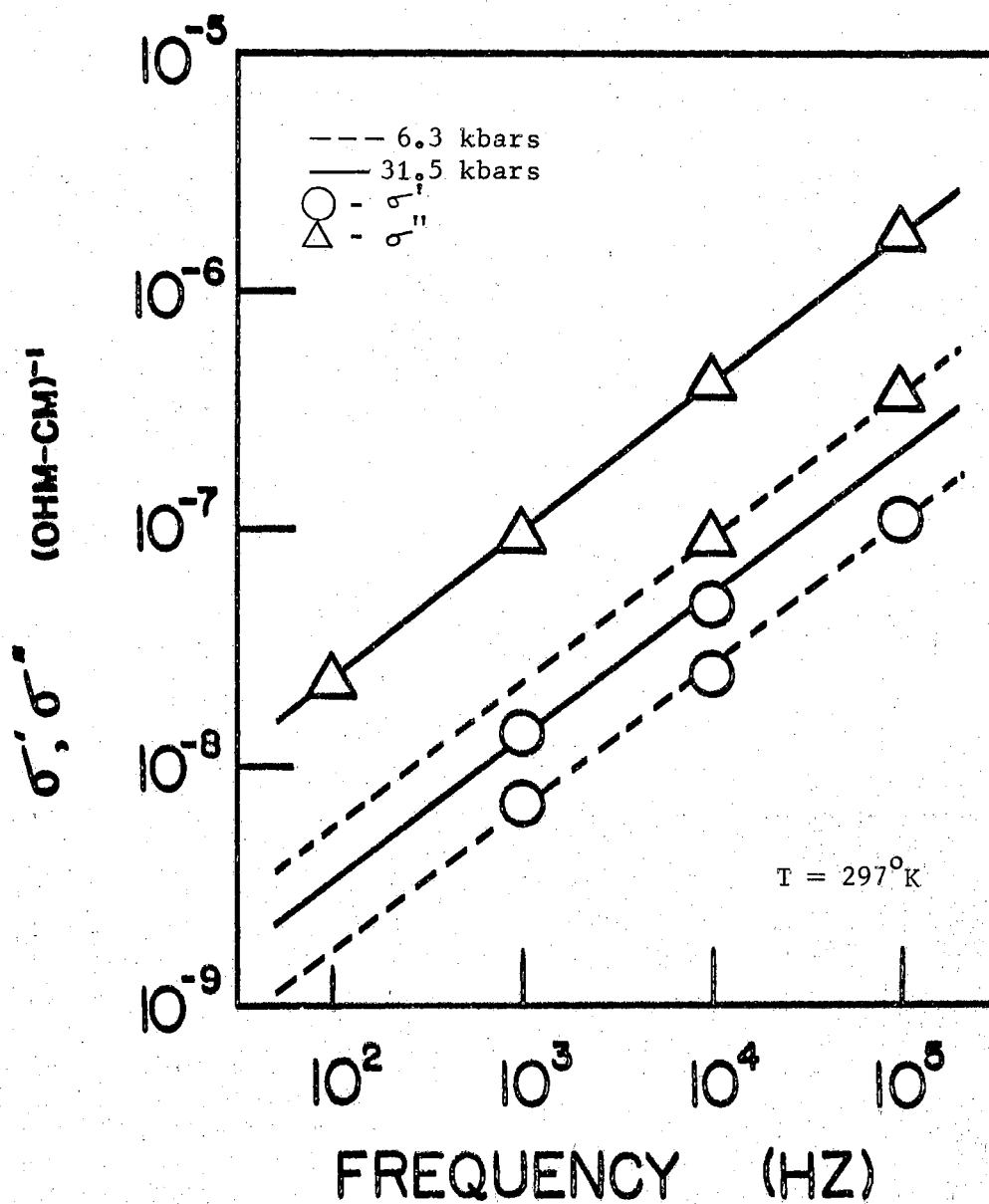
Figure 19. The Real σ' and Imaginary σ'' Parts of the Complex Conductivity for the Acridone-MTA Polymer as a Function of Frequency
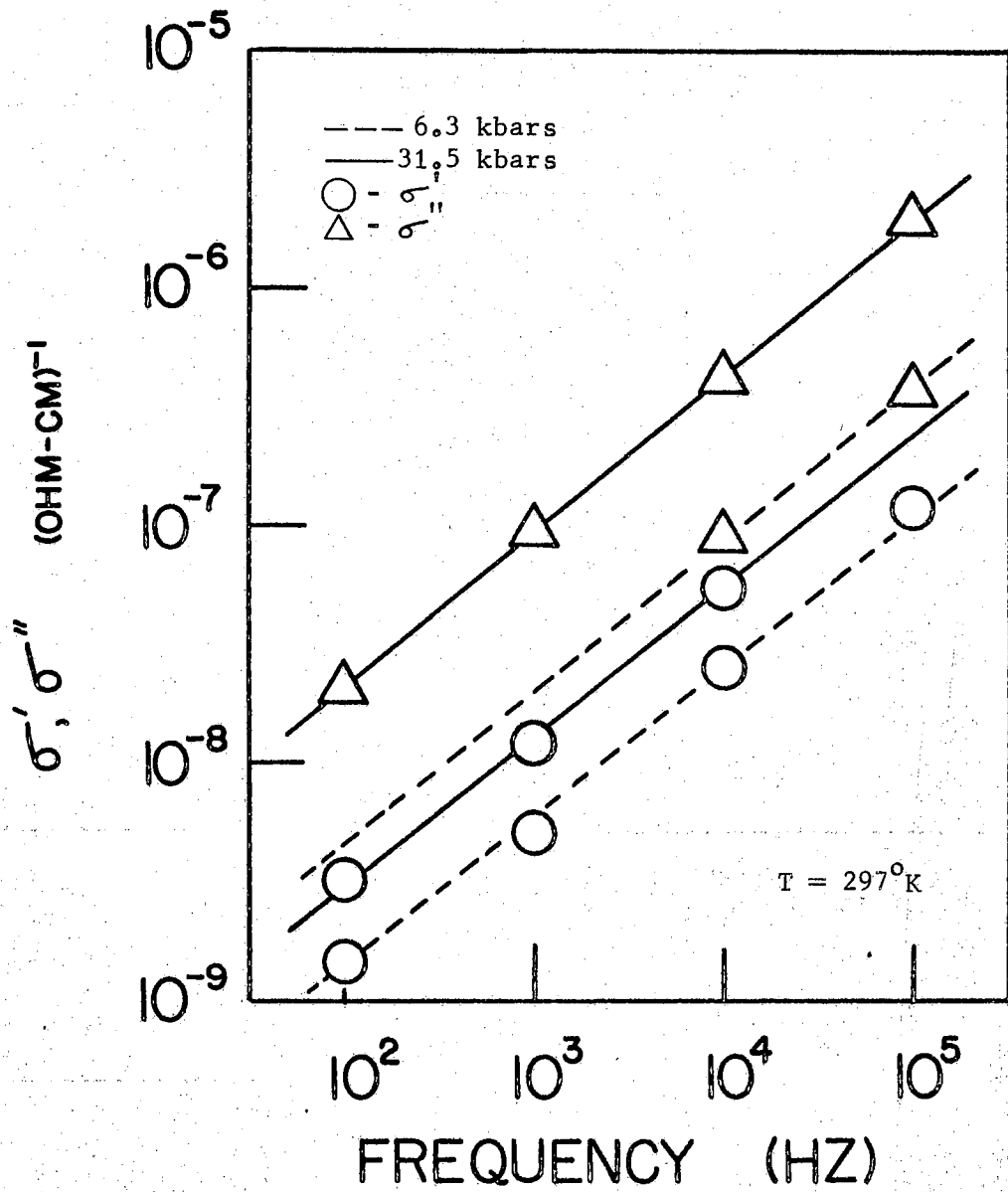
Figure 20. The Real σ' and Imaginary σ'' Parts of the Complex Conductivity for the Acridone-PMA Polymer as a Function of Frequency
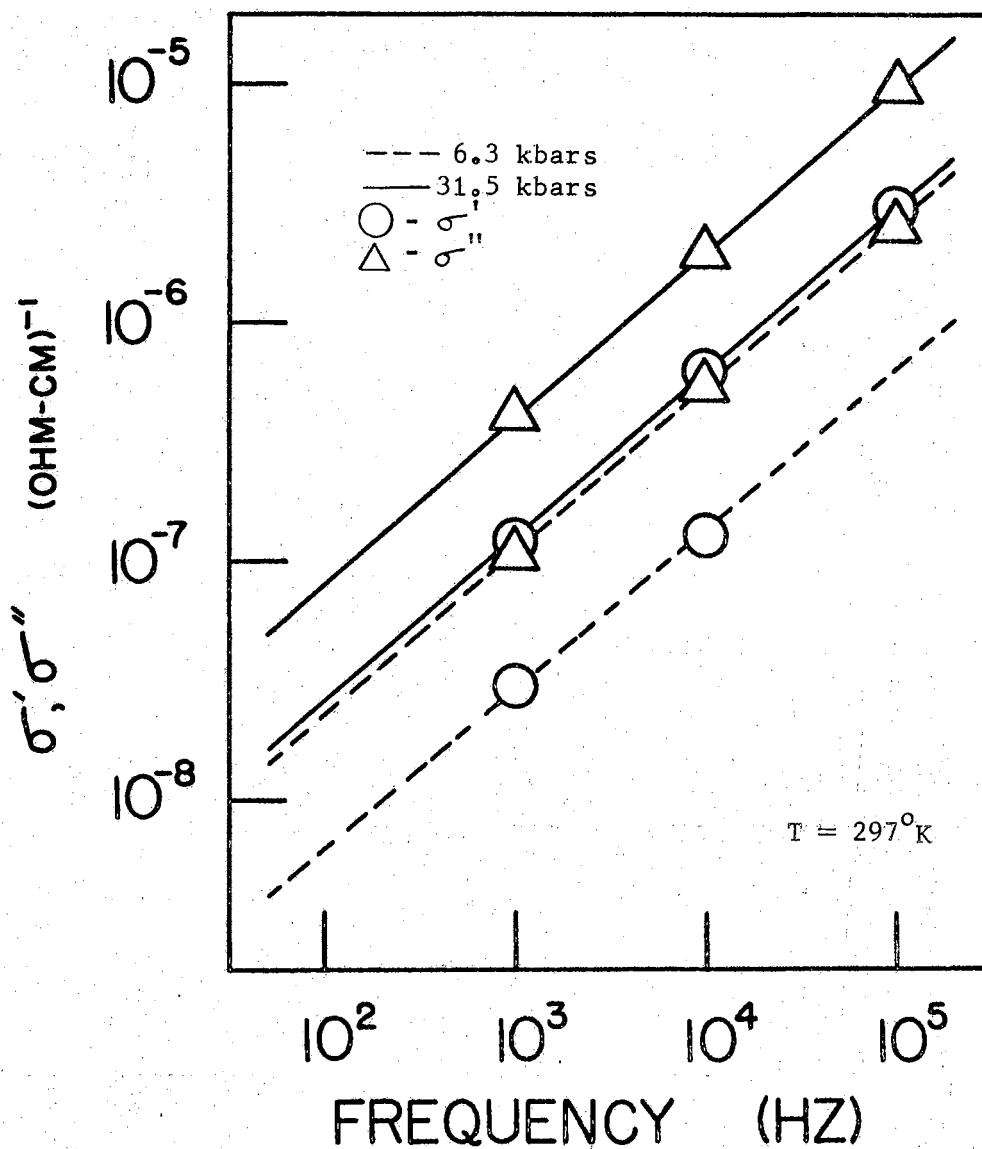
Figure 21. The Real σ' and Imaginary σ'' Parts of the Complex Conductivity for the Phenanthrene-PMA Polymer as a Function of Frequency

The values of s , the predicted values of $\tan(\tfrac{1}{2}s\pi)$, and the experimental values of $\tan(\tfrac{1}{2}s\pi)$ are shown in Table X for the seven polymers. The results indicate the values of s are not identical for the frequency range, but differ only slightly. For all cases the value of the permittivity was higher than the value predicted from the a. c. conductivity using equation (44).

Argall and Jonscher (169) have suggested another relation for the total conductivity,

$$\sigma = (\epsilon - \epsilon_\infty) \sin \left[(1-a)(\pi/2) \right] \mathcal{J}_\alpha^{a-1} \omega^a + \sigma_{DC} + \sigma_{AC}(\omega) \tag{45}$$

where a is the temperature dependent distribution factor and $\mathcal{J}_\alpha$ is some average relaxation time. This relation implies a Debye type dispersion distinct from the conduction loss mechanism. For different frequencies, either the first or last term will dominate. The frequency-dependent conductivity due to an electronic hopping mechanism is dominant at the high frequencies but not necessarily at the lower frequencies.

A simple model has been developed to give semi-quantitatively a picture of the field frequency dependence of the permittivity (170). The permittivity depends directly on the number of dipoles or macropole pairs, and the field reorganization of macropole clusters is controlled by electrostatic interactions or the reciprocal of the local permittivity. The results predict that the number of favorably aligned macropoles is proportional to $\omega^{-\frac{1}{2}}$. The values of s obtained here are in fair agreement and average about 0.5. The values of s for silicon, as obtained by Pollak and Geballe (167), and for germanium, as obtained by Golin (168), were approximately 0.75.

TABLE X

THE MEASURED AND CALCULATED VALUES OF TAN $(\frac{1}{2}\pi s)$

Sample	s	tan $(\frac{1}{2}\pi s)$ from measured values of s	tan $(\frac{1}{2}\pi s)$ calculated from $(\epsilon_r \epsilon_o \omega/\sigma')$	
			P=31.5kb	P=6.3kb
Thianthrene-PMA	0.39	0.70	11.	4.3
Thianthrene-MTA	0.47	0.90	17.	23.
Dibenzofuran-PMA	0.48	0.94	8.5	6.0
Xanthone-PMA	0.48	0.95	5.9	3.7
Acridone-MTA	0.61	1.44	7.8	3.3
Acridone-PMA	0.66	1.65	7.1	3.2
Phenanthrene-PMA	0.70	1.91	3.1	3.8

Molecular Length

For the conducting polymers investigated here the normal methods
for determining average molecular length cannot be employed. As the
PAQR's are insoluble, viscometric molecular length measurements could
not be made. A method suggested by Rosen and Pohl (1) utilizes the
d. c. field effect to determine the molecular length. The external
electric field across the molecule gives energy or lowers the activa-
tion energy required to create carriers.

Using the simple square well potential model for a one-dimensional
group of molecules, the external field will cause the potential wells
to slant. Each well represents the projected length of the molecule in

the direction of the field. Then the potential of the ith well is decreased by the amount

$$\phi_i = \vec{\mathcal{E}} \cdot \vec{L}_i \qquad (46)$$

where $\vec{\mathcal{E}}$ is the applied field as seen locally by the ith molecule and $\vec{L}_i$ is the length of the ith molecule. Then the projected length of the ith molecule in the direction of the external field is given by,

$$\vec{L}_i = L \cdot \cos \Theta_i \qquad (47)$$

where L is the length of the molecule and Θ_i is the angle between the field direction and the orientation of the ith molecule. Then the effective carrier activation energy gap is given by

$$E = E_g - |e|\phi_i = E_g - |e|\mathcal{E}L \cos\Theta_i \qquad (48)$$

where e is the electronic charge, and the carrier concentration is given by

$$n = \sum_{\Theta_i} n_{o_i} \exp\left[\frac{(-E_g + |e|\mathcal{E}L \cos\Theta_i)}{2kT}\right]. \qquad (49)$$

Then assuming random distribution of orientations,

$$n = \frac{2kTn_o}{|e|\mathcal{E}L}\left(\exp\left[\frac{|e|\mathcal{E}L}{2kT}\right] - 1\right) \exp\left[-\frac{E_g}{2kT}\right], \qquad (50)$$

and for constant temperature,

$$\left(\frac{\sigma}{\sigma_o}\right)_{T,P} = \frac{2kT}{|e|\mathcal{E}L}\left(\exp\left[\frac{|e|\mathcal{E}L}{2kT}\right] - 1\right) \qquad (51)$$

where σ_o is the conductivity at zero field intensity. Equation (51) predicts the conductivity to be a function of electric field intensity and molecular length at a constant temperature. It is assumed that the external field applied is the same as the local field which produces the effect. It is further assumed that the carrier mobility is not appreciably affected by the change in electric field. Another important assumption is the condition of random molecular orientation, even though the sample is measured under uniaxial pressure. It would appear possible that after the sample has been recycled several times to high pressure, some non-random alignment would occur. The change in pressure did not alter the d. c. or a. c. conductivity field effect (see Figure 13). It should be noted here also that the a. c. and d. c. conductivity field effects were the same for low frequencies where the a. c. conductivity was essentially the same as the d. c. conductivity, since the hopping process was negligible compared to the d. c. mechanism.

Equation (51) can be approximated for low fields by the equation

$$\frac{\sigma}{\sigma_o} = 1 + \left(\frac{|e| L}{4 k T}\right) \mathcal{E} \, . \tag{52}$$

Then

$$\frac{\sigma}{\sigma_o} - 1 = \left(\frac{|e| L}{4 k T}\right) \mathcal{E} \, . \tag{53}$$

One can easily determine the molecular length when $(\sigma/\sigma_o - 1)$ is plotted as a function of $\mathcal{E}$ on a log-log scale. The average molecular length can then be found by shifting a single curve along the $\mathcal{E}$ axis. The slope of $(\sigma/\sigma_o - 1)$ as a function of $\mathcal{E}$ is approximately equal to 1 and the intercept is proportional to the molecular length.

If Joule heating is causing the field effect, the slope of $(\sigma/\sigma_o - 1)$

as a function of $\mathcal{E}$ will be approximately equal to 2, since the effect is proportional to $\mathcal{E}^2$. By plotting the results in this manner, the valid data can be determined and the model can be applied to determine the molecular length.

The results for ten samples for which the theoretical model can be applied are shown in Figures 22 and 23. Twenty-five more samples were also measured, but the results did not show the linear field dependence necessary to determine the molecular length. It was concluded that the field intensities necessary to produce the molecular length field effect exceeded the limiting values of the Joule heating effect for these samples. Table XI gives the molecular lengths by d. c. field effect measurements and by the electron spin resonance measurements. The ESR results are always greater than d. c. field effect results. This may be explained by the fact that the ESR method measures the total length of the molecule while the d. c. field method measures the distance between the extremities of the molecule. Thus, if the molecule were a straight rod, the two measured lengths would be identical. However, a more realistic picture would suggest overlapping and switchbacks of the backbone of the molecule, making the total length much longer than the extremities of the molecule. The ratio of the two values might then suggest the amount the molecule has been stretched out or its approach to being rod-shaped.

Molecular Length via Homologous Series

In order to relate the electrical properties such as conductivity and permittivity to the molecular length, a series of polymers was prepared in which the reactants and polymerization technique were identical
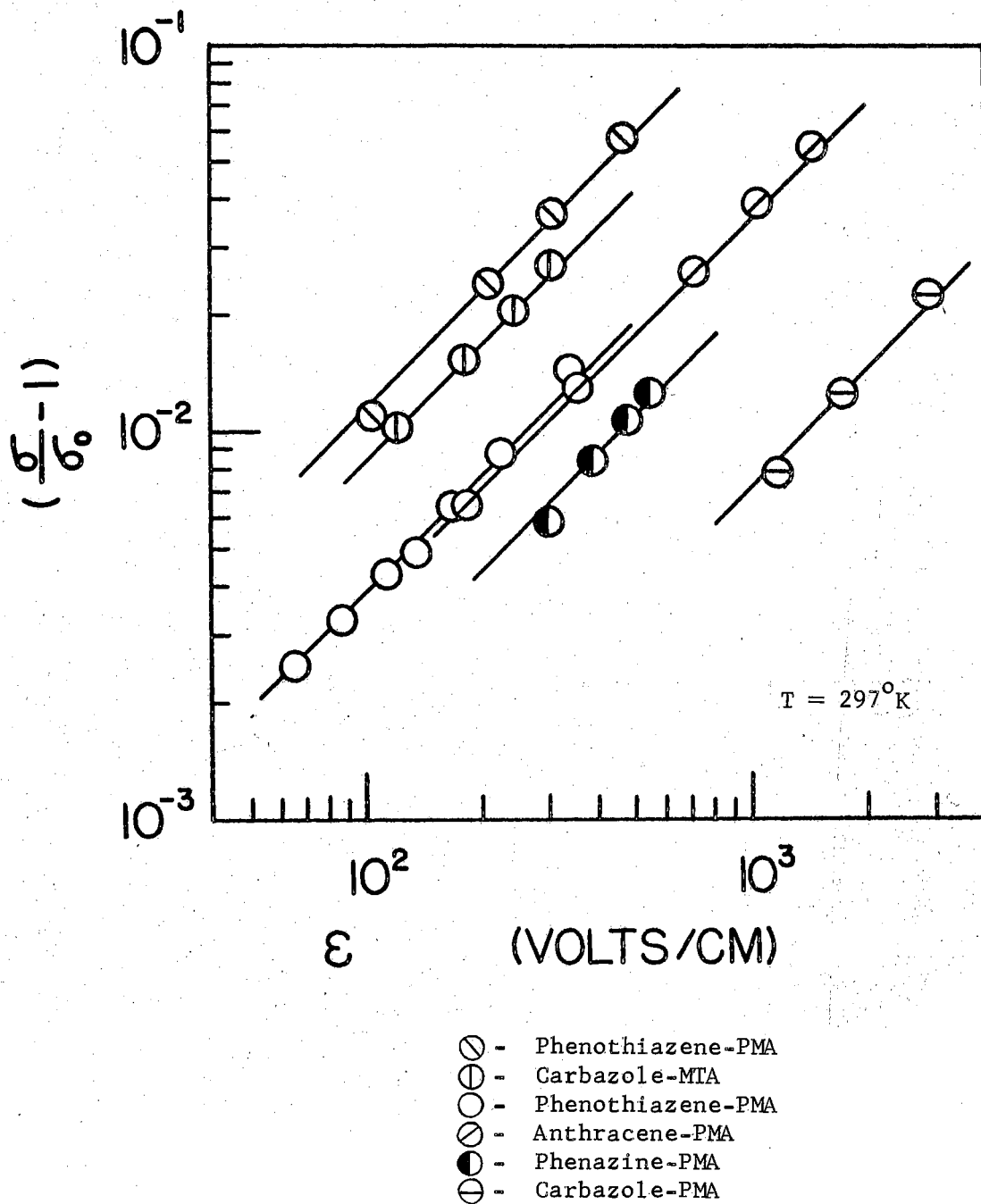
Figure 22. The Value of $(\sigma/\sigma_o - 1)$ as a Function of the Field
Intensity $\mathcal{E}$ for Six PAQR Polymers

Figure 23. The Value of $(\sigma/\sigma_0 - 1)$ as a Function of the Field Intensity ε for Four PAQR Polymers

but the reaction times were changed. The mole ratio of pyrene, pyro-
mellitic dianhydride and zinc chloride was 1 : 1 : 2 and the reaction
temperature was $306^{\circ}C$. The reactants were heated under nitrogen atmos-
phere for one to thirty hours and then ground and thoroughly extracted
in the same manner as the PMA polymers described in Chapter II. The
results for the d. c. conductivity and permittivity at 1000 Hz are shown
in Table XII.

TABLE XI

ESTIMATED MOLECULAR LENGTHS

Sample	L_{dc} ($\overset{o}{A}$)	L_{esr} ($\overset{o}{A}$)
Phenothiazene-PMA-1	1300	1465
Carbazole-MTA	1000	--
Phenothiazene-PMA-2	460	702
Anthracene-PMA	420	4369
Dibenzofuran-PMA	340	1168
Phenoxathiin-PMA	275	1003
Phenazine-PMA	270	--
Xanthene-PMA	240	1721
Fluorene-PMA	105	2482
Carbazole-PMA	88	1415

TABLE XII.

REACTION TIME, CONDUCTIVITY, RELATIVE PERMITTIVITY FOR
PYRENE-PMA POLYMERS AT A PRESSURE OF 1.6
KILOBARS AND TEMPERATURE OF 297°K

Reaction Time (Hrs)	σ_{dc} (ohm-cm)$^{-1}$	ϵ_r (1000 Hz)
1	1.02×10^{-5}	97
4	3.23×10^{-5}	260
8	3.73×10^{-5}	392
30	1.23×10^{14}	489

The samples were quite conductive and showed an increase in conductivity and permittivity as the reaction time increased. These results indicate that the polymerization, i.e. the molecular length, and hence the conductivity, increased with reaction time, as would be expected from theory.

Several other similar series were prepared using violanthrone with iodobenzoic and chlorobenzoic acid heated to 306°C in the presence of zinc chloride, but little if any reaction took place, since the solubility and electrical properties were essentially the same as for pure violanthrone, and the reaction mix never showed signs of fusion. Violanthrone did react, however, with pyromellitic dianhydride at 445°C, the boiling point of sulfur. The conductivity of the starting reactant was increased from 4×10^{-11} to 3×10^{-5} mho/cm. This increase in conductivity indicated that some polymerization took place.

An attempt was made by P. Clark to polymerize pyrene and pyromel-litic dianhydride in an $AlCl_3$-NaCl melt at 140°C to examine the conduc-tivities of samples reacted for various times. However, the reaction melt stayed liquid for only about 1.5 hours, then solidified, preventing fractional samples from being taken for longer periods. It was found, however, that the reaction could be run in a large excess of nitroben-zene at temperatures below 125°C for extended periods of time. The sam-ples obtained ranged in color from yellow (the first five samples, taken over a two-hour period) to black later on. When these samples were tes-ted for conductivity, they yielded the unexpected results shown in Fig-ure 24.

It is clear that the conductivity had gone through a maximum at an early stage, and that prolonged reaction then caused a decrease in the conductivity contrary to expectation. Pure pyrene has a conductivity in the order of 10^{-20} mho/cm. It is as if "over-reaction" had somehow spoiled the molecular planarity, etc., necessary for ekaconjugation. Similar results had appeared before for polyacenequinone radical poly-mers, when attempts were made to correlate polymerization time with con-ductivity. It seems reasonable to suspect the catalytic system of car-rying on only partially toward the desired degree of ekaconjugated poly-merization, and concurrently producing competing reactions which reduced the effectiveness of the resultant molecular structure for electronic conduction.

Three polybenzimidazophenanthroline (BBB) polymers were furnished by R. L. Van Deusen of the Air Force Materials Laboratory. The intrin-sic viscosity in H_2SO_4 and the structure of each polymer were also provided. Before measurement the samples were dried by extraction with
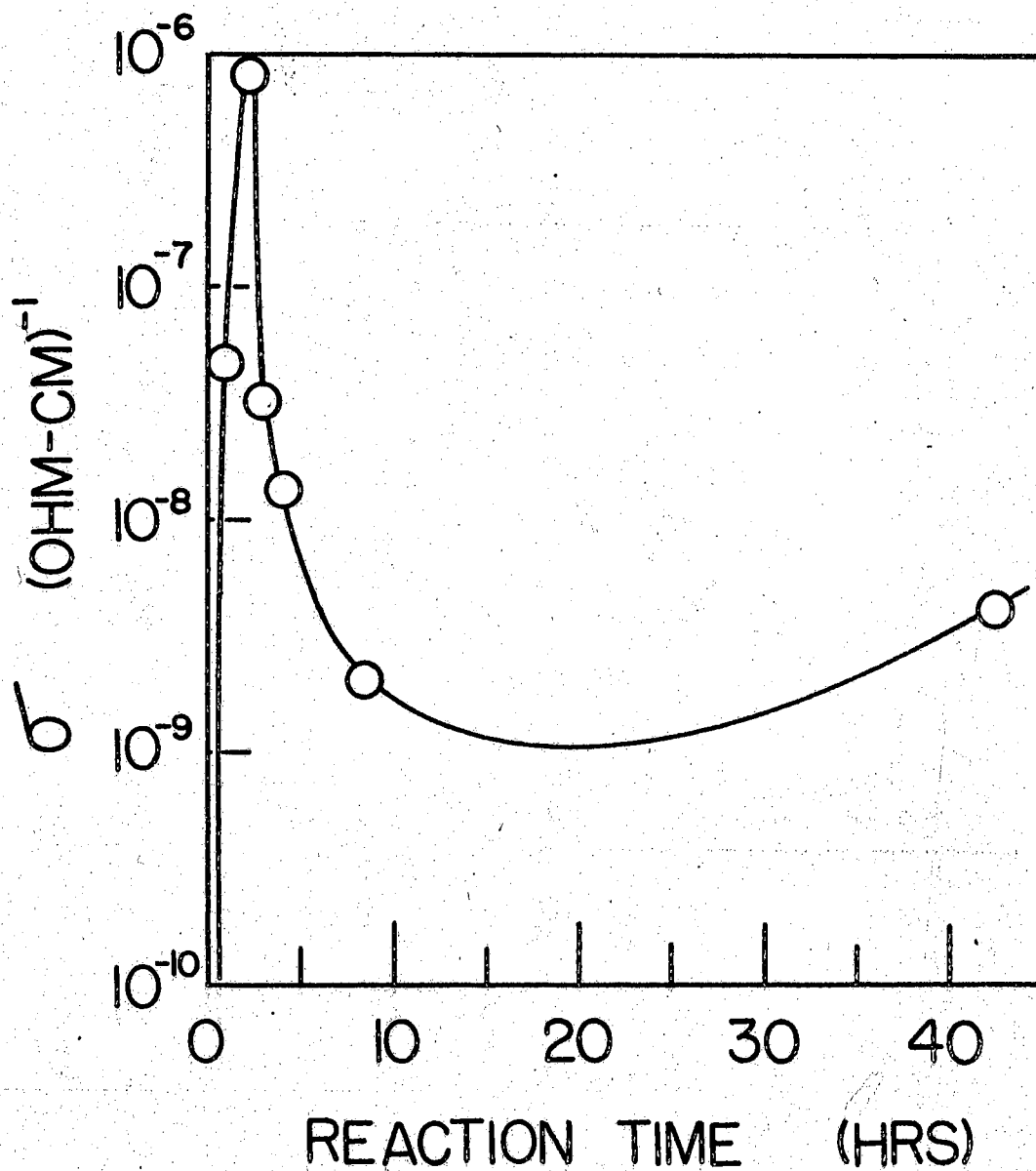
Figure 24. The Conductivity at Zero Pressure as a Function of
Reaction Time for the Pyrene-PMA Polymers Poly-
merized at 125°C in Nitrobenzene with AlCl$_3$

boiling methanol. The samples were then sheared under pressure and micro-ground and extracted again with boiling methanol. Many attempts were made to obtain reproducible conductivity results for the three polymer samples. No reliable results were obtained, and it was concluded that the samples were charge transfer complexes rather than eka-conjugated polymers. The samples were stirred in solutions of 5 per cent hydrochloric acid at room temperature for a period of seven days. Each day the samples were rinsed and placed in a new solution. After the seven days the samples were thoroughly rinsed with methanol and placed in a $50^{\circ}C$ oven overnight. The acid removed the H_2SO_4 from the samples and thus restored the necessary eka-conjugation. The results are presented in Table XIII. The conductivity increases with the increasing intrinsic viscosity, and thus with molecular length, as expected from theory.

TABLE XIII

THE CONDUCTIVITY AT ZERO PRESSURE AND ROOM TEMPERATURE AND THE
INTRINSIC VISCOSITY IN H_2SO_4 FOR THE BBB POLYMERS

Sample	$[\eta]$	$\sigma_{P=0}$ (mho/cm)
VG-20-25	0.80	2.45×10^{-7}
M-BBB-3	1.72	2.85×10^{-7}
M-BBB-1	2.54	2.20×10^{-5}

Chemical Structure

The chemical structure of the monomer unit also affects the degree of hyperelectronic polarization and the conductivity. A large variety of polymers has been measured by Kho and Pohl (140) to determine the influence of chemical structure on the conduction properties of polymers. They concluded that as the number of fused rings in the hydrocarbon portion was increased, the conductivity increased; and as the ionization constant of the acid monomers increased, the conductivity also increased. The activation energy interval and pressure coefficient decreased as the number of fused rings in the hydrocarbon portion increased. All of these conclusions agree with the basic model of electronic conduction.

The influence of chemical structure can also be shown from the series of pyromellitic dianhydride polymers prepared by J. Mason and described in Chapter II. Here the number of fused rings of the hydrocarbon portion remains constant. The hydrocarbon portion is modelled as shown in Figure 25(A), where X or Y can be S, O, CH_2, C=O or NH. Another form of the hydrocarbon portion is shown in Figure 25(B), where X can be S, O, CH_2, C=O or NH. The conductivities and number of spins/g have been determined for each sample and the results are presented in Table XIV, in order of decreasing conductivity. The values of s for several samples are also given. The increase in the value of s indicates a decrease in the permittivity, as seen in the previous section. The number of spins/g also decreases as the conductivity decreases. Pohl and Chartoff (124) observed that the number of spins/g was proportional to the one-fifth power of the conductivity. The results here suggest a similar relation.
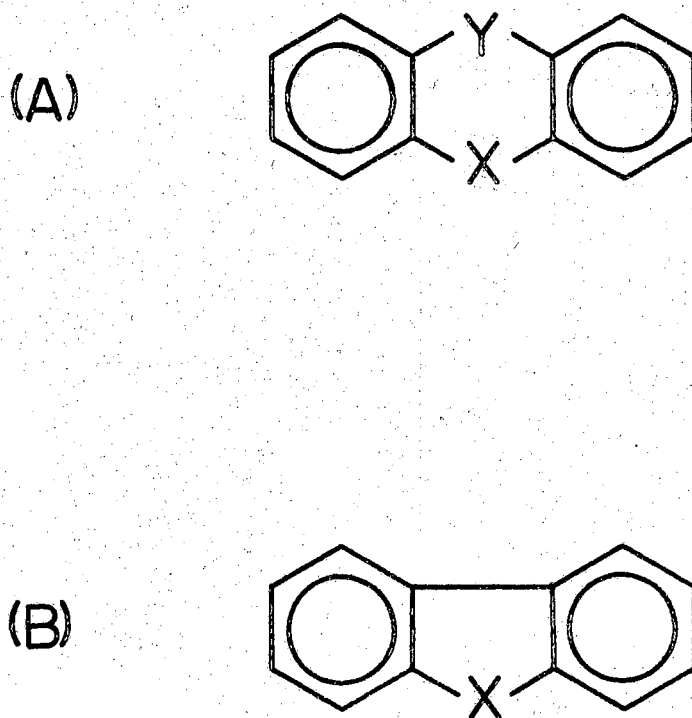
Figure 25. Diagram of the Hydrocarbon Portion of PAQR
Polymers Showing (A) X and Y Substitution
Positions, and (B) the Single Substitu-
tion Position X

TABLE XIV

ELECTRICAL PARAMETERS AND CHEMICAL STRUCTURE
OF PMA POLYMERS

Sample	X	Y	σ^{*} (mho/cm)	ρ^{**} (spins/g) $(x10^{-19})$	s, frequency exponent
Anthraquinone-PMA	C=O	C=O	$1.14x10^{-5}$	20.4	
Phenothiazine-PMA	S	NH	$3.57x10^{-6}$	19.0	
Thianthrene-PMA	S	S	$2.78x10^{-7}$	17.8	0.39
9-Thioxanthene-PMA	S	CH$_2$	$1.61x10^{-7}$	17.7	
Dibenzothiophene-PMA	--	S	$9.09x10^{-8}$	18.7	
Carbazole-PMA	--	NH	$9.09x10^{-8}$	13.2	
9-Thioxanthane	S	C=O	$9.09x10^{-9}$	9.95	
Dibenzofuran-PMA	--	O	$9.09x10^{-9}$	19.8	0.48
Phenoxathiin-PMA	S	O	$8.33x10^{-9}$	21.8	
9,10-Dihydroanthra-cene-PMA	CH$_2$	CH$_2$	$8.33x10^{-9}$	9.25	
Phenoxazine-PMA	O	NH	$5.26x10^{-9}$	23.9	
Xanthone-PMA	O	C=O	$2.56x10^{-9}$	14.1	0.48
Acridan-PMA	NH	CH$_2$	$1.00x10^{-9}$	11.3	
Xanthene-PMA	O	CH$_2$	$6.25x10^{-10}$	10.7	
9-Fluorenone-PMA	--	C=O	$4.35x10^{-10}$	4.24	
Acridone-PMA	C=O	NH	$2.86x10^{-10}$	8.30	0.66
Fluorene-PMA	--	CH$_2$	$2.86x10^{-11}$	7.50	

*Pressure = 0; T = 25°C   **T = 25°C

From these results it can be seen that the polymers containing S in the X or Y position are the most conductive, while those polymers containing CH_2 are the least conductive. Table XV generalizes the results.

TABLE XV

CONDUCTIVITY RANGE FOR DIFFERENT SUBSTITUTION ELEMENTS

X or Y	Conductivity Range (mho/cm)
S	$10^{-8} - 10^{-6}$
O	$10^{-9} - 10^{-8}$
CH_2	$10^{-11} - 10^{-9}$
C=O	$10^{-10} - 10^{-5}$
NH	$10^{-10} - 10^{-6}$
--	$10^{-11} - 10^{-7}$

A computer program, provided by P. Clark, was used to make quantum mechanical calculations employing Hückel method. Figure 26 shows the model with atomic site numbers for the calculations of the hydrocarbon and pyromellitic dianhydride monomer unit. The input for each calculation was the same except for the X and Y positions corresponding to atomic site numbers 6, 25, 13 and 26. The program output gave results for the LEMO and HOMO energies, the energy difference in units of β,

85

Figure 26. Molecular Model Used for
Hückel Calculations Showing
Atomic Site Numbers
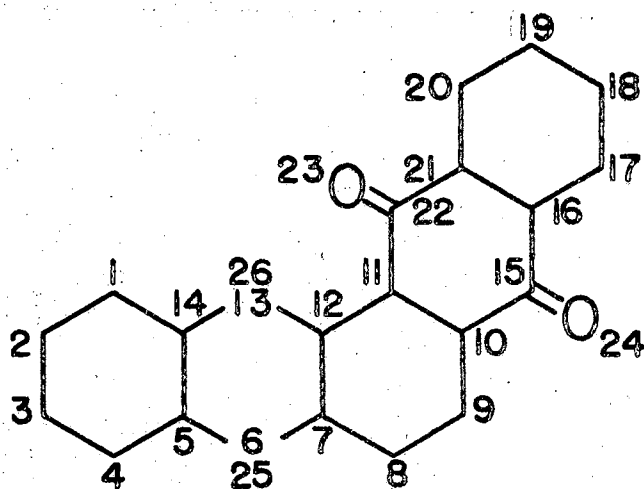
Figure 26. Molecular Model Used for
Hückel Calculations Showing
Atomic Site Numbers

the electron and charge densities for each atomic site and the bond orders and bond lengths. The HOMO-LEMO energy differences are listed in Table XVI, where β was 1.60 eV, as known for benzene. Figure 27 shows the energy difference as a function of conductivity for PMA polymers. There is a distinct separation in the results at 10^{-7} (ohm-cm)$^{-1}$. Samples with conductivities of 10^{-11} to 10^{-7} (ohm-cm)$^{-1}$ have HOMO-LEMO values of 0.0 - 0.2 eV, and samples with conductivities of 10^{-8} to 10^{-5} (ohm-cm)$^{-1}$ have HOMO-LEMO values of 0.5 - 1.0 eV. The high conductivity polymers show a general decrease in conductivity as the HOMO-LEMO energy difference increases. Figure 28 shows a similar separation for the number of unpaired spins as a function of the calculated HOMO-LEMO energy difference. Figures 29 and 30 show the conductivity energy intervals and spin activation energies plotted as a function of the HOMO-LEMO energy difference for the same series of polymer samples. The HOMO-LEMO energy level difference does not seem to correlate too well with the observed energy interval for conduction, which is surprising since the conductivity is related to the energy interval; i. e. the conductivity increases with decreasing energy interval. The electron spin resonance activation energy values do not correlate with the HOMO-LEMO energy level difference either. The reasons for this are not clear.

For this series of polymers, there was no control of molecular length except for the constant reaction time. Thus the elemental components contained in the hydrocarbon portion may control the polymerization rate, and thus the conductivity. For example, the hydrocarbon portion containing sulphur may permit more monomer units to join and remain stable than the hydrocarbon portion containing CH_2. The chemical structure as investigated here may thus influence only the molecular

length, rather than affecting the conductivity directly through mobil-
ity or carrier concentration.

TABLE XVI

THE CALCULATED HOMO-LEMO ENERGY DIFFERENCE
FOR PMA POLYMERS

| Sample	X	Y	ΔE (eV) (HOMO-LEMO)
Anthraquinone-PMA	C=O	C=O	0.690
Phenothiazine-PMA	S	NH	0.963
Thianthrene-PMA	S	S	0.808
9-Thioxanthene-PMA	S	CH_2	0.195
Dibenzothiophene-PMA	--	S	0.014
Carbazole-PMA	--	NH	1.067
9-Thioxanthane-PMA	S	C=O	0.125
Dibenzofuran-PMA	--	O	0.134
Phenoxathiin-PMA	S	O	0.146
9,10-Dihydroanthracene-PMA	CH_2	CH_2	0.145
Phenoxazine-PMA	O	NH	1.243
Xanthone-PMA	O	C=O	0.200
Acridan-PMA	NH	CH_2	0.147
Xanthene-PMA	O	CH_2	0.149
9-Fluorenone-PMA	--	C=O	0.016
Acridone-PMA	C=O	NH	0.062
Fluorene-PMA	--	CH_2	0.158
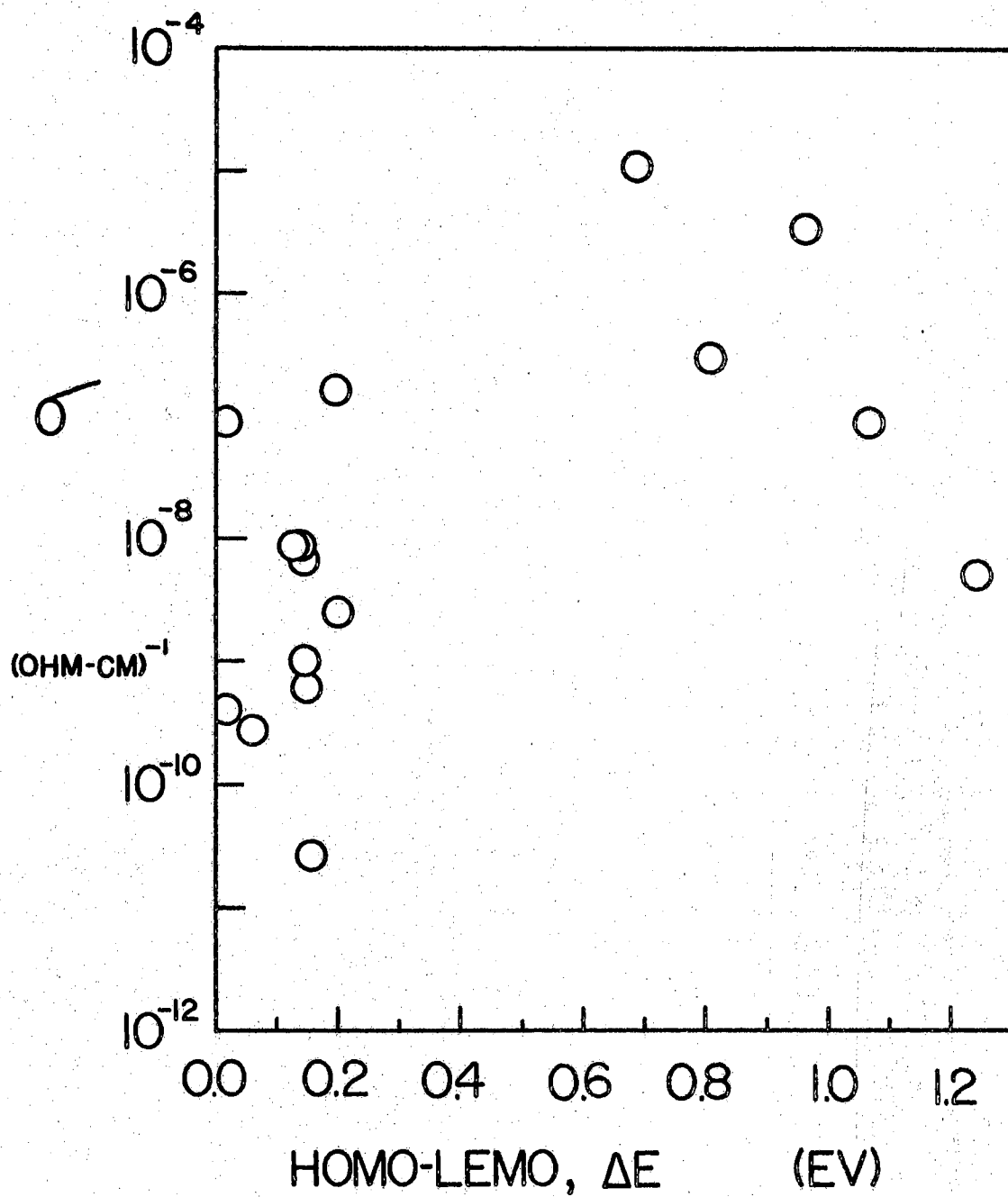
Figure 27. The D. C. Conductivity at Zero Pressure and 297°K as a Function of the Calculated HOMO-LEMO Energy Difference for the PMA Series
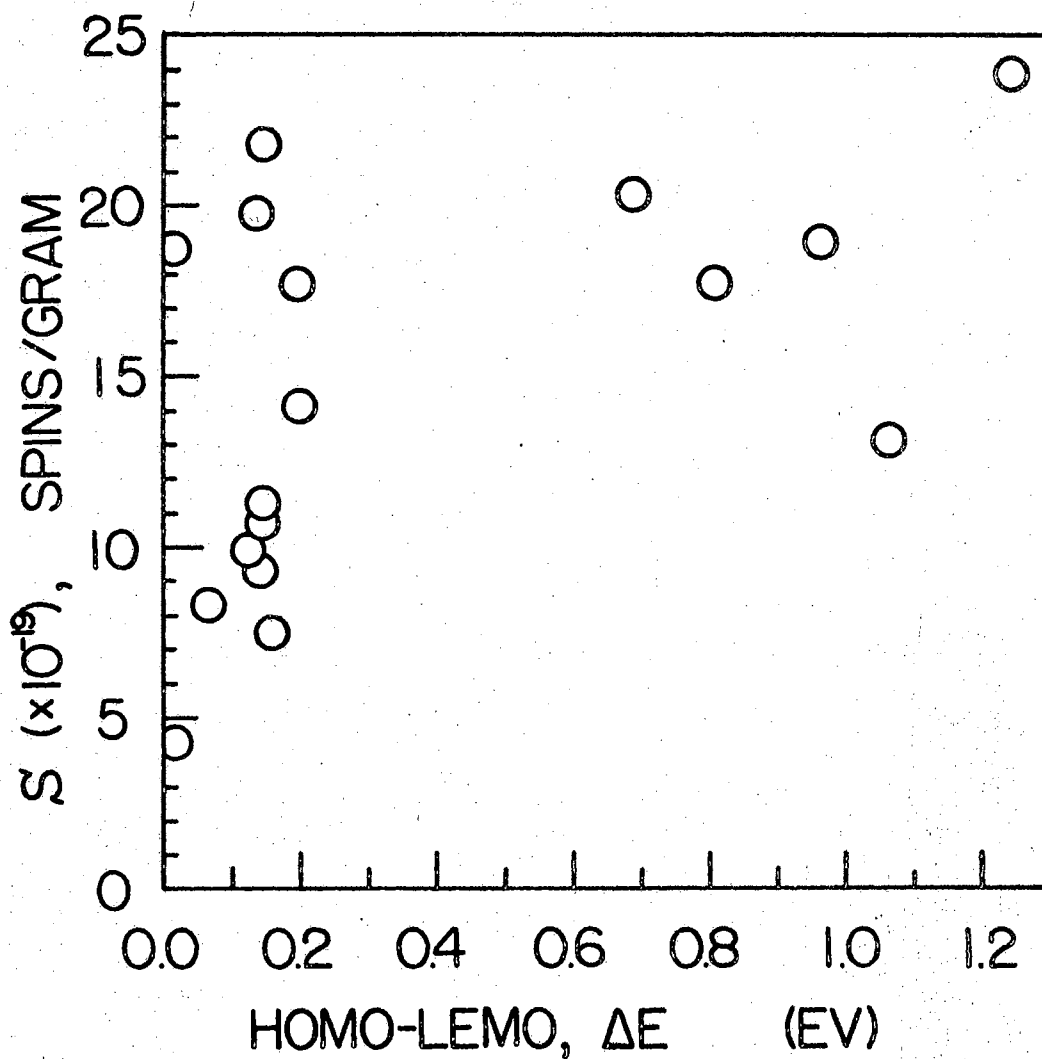
Figure 28. The Number of Spins/g at 297°K as a Function of the
Calculated HOMO-LEMO Energy Difference for the PMA
Series
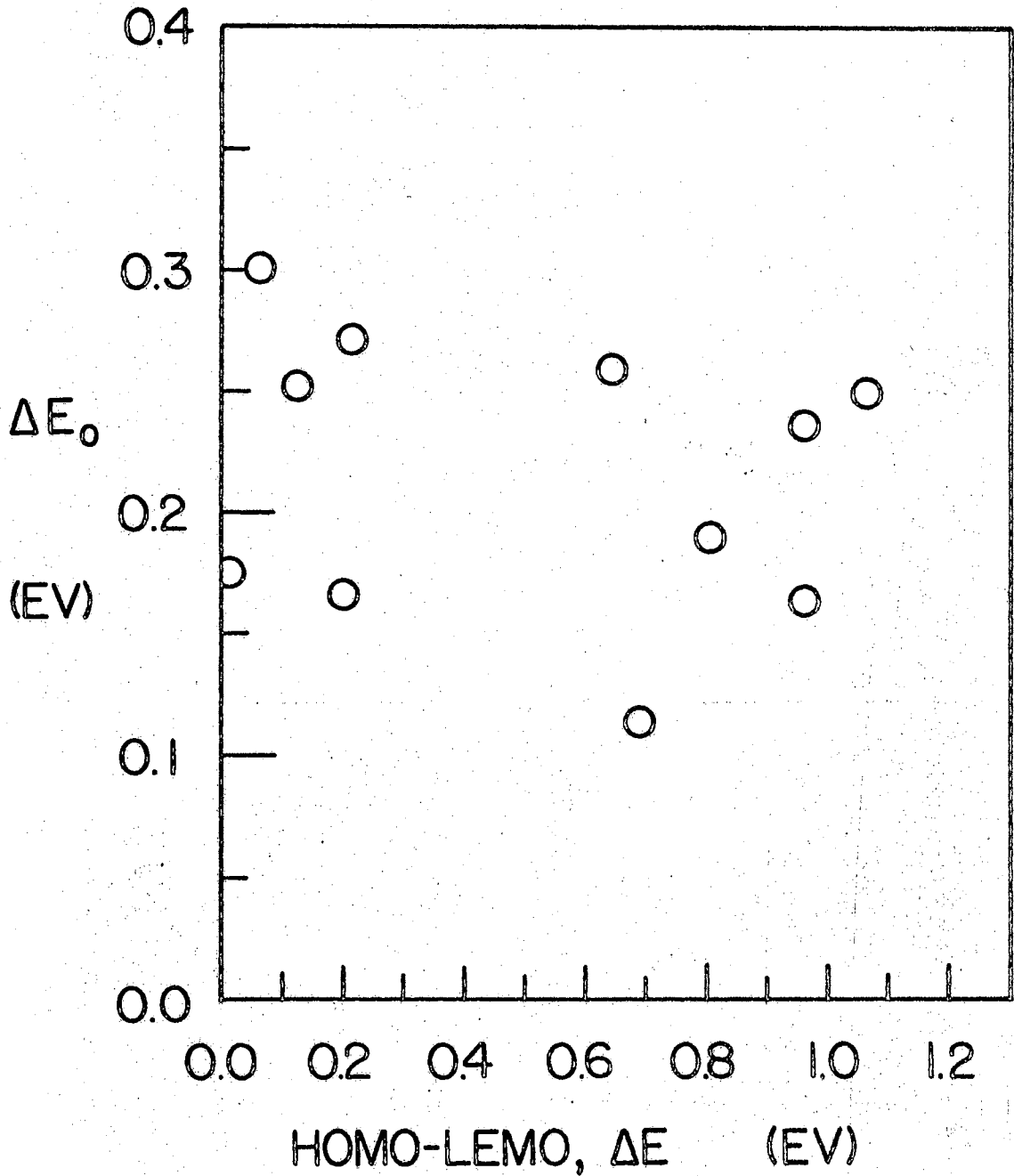
Figure 29. The D. C. Conductivity Energy Interval at Zero Pressure as a Function of the Calculated HOMO-LEMO Energy Difference for the PMA Series.
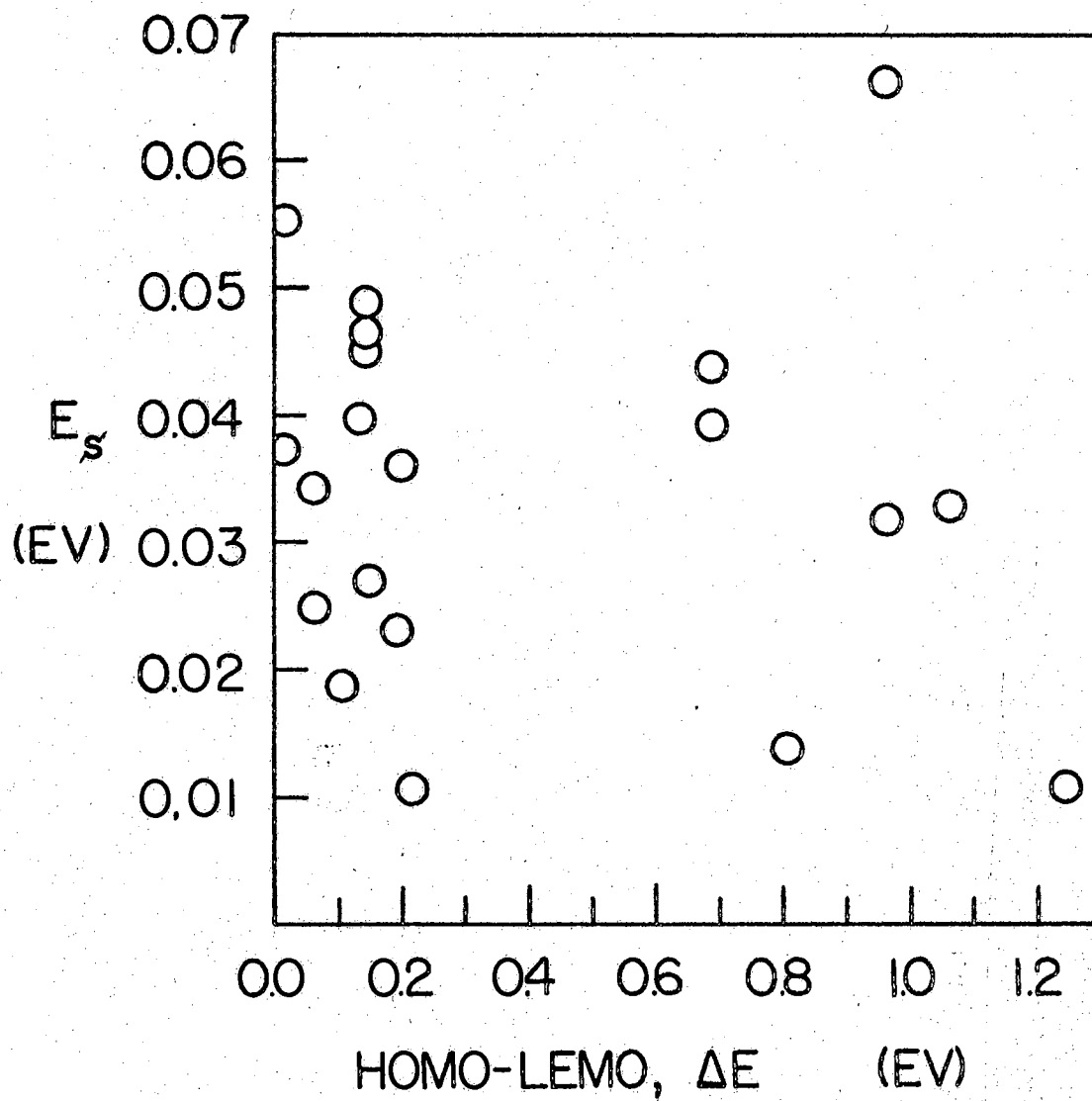
Figure 30. The Spin Activation Energy as a Function of the Calculated HOMO-LEMO Energy Difference for the PMA Series

CHAPTER IV

CONCLUSIONS AND SUGGESTIONS FOR FURTHER STUDY

Model for Hyperelectronic Polarization

A quantitative model has been experimentally developed for hyper-electronic polarization and the associated conductivity mechanisms. The permittivity and conductivity responses have been well defined for pressure, temperature, external electric field intensity and frequency.

From the discussions in Chapter III, the results can be generalized into three categories: (a) the production or number of active macropoles and carriers, (b) the behavior of the macropoles and carriers in the external field, and (c) the intrinsic structure of the organic polymer.

The pressure and temperature have the greatest influence on the creation and total number of active polarizing macropoles which exhibit hyperelectronic polarization and on the carriers which contribute the main portion of the measured conductivity. The energy interval, defined by the response to temperature, is essentially the same for macropoles and carriers at normal temperatures. This implies that the same average energy is required to create the Mott excitons or electron-hole pairs on different molecules, and the carriers or the unassociated electrons and holes. In the a. c. field macropoles and carriers are related and the number of each type is controlled by the frequency. At high frequencies the macropoles become a. c. carriers if they cannot keep up

with the polarizing field. At low frequencies the total conductivity is essentially the same as the d. c. conductivity. Here the energy interval is also the same for the permittivity and conductivity.

The pressure controls the molecular orbital overlap and thus the energy required to transfer charge between molecules. The total pressure coefficient for the permittivity and conductivity decreases as the frequency increases. This is to be expected from this model since the probability of transition between molecules decreases as the frequency increases, since the electron does not have sufficient time to make the transition. The total permittivity pressure coefficient is always less than the conductivity pressure coefficient and decreases more rapidly as the frequency increases. This would also be expected from the model since the transition rate between molecules would affect only the total number of polarizing macropoles. The transition rate affects both the number of carriers and the mobility associated with the activation energy, and thus the number of macropoles and carriers is the same for the permittivity and conductivity.

The calculated potential well model has been suggested to interpret the permittivity field intensity response. The polarizing charge moves in a potential well defined by equation (26) in Chapter III. This equation predicts almost free movement of the charge between the two potential barriers of a one-dimensional potential box. The predicted dimensions of the box agree well with x-ray diffraction results.

The frequency response of the permittivity and a. c. conductivity suggests the application of the hopping model developed by Pollak and Geballe (167). The observed hyperelectronic polarization is the out-of-phase or imaginary component of the complex conductivity. The

Kramers-Kronig relation can be used to approximate the permittivity if the a. c. conductivity is known. This does not directly imply a relation between the d. c. conductivity and the observed permittivity, although for the samples measured here the a. c. conductivity is generally proportional to the d. c. conductivity. The samples measured in this investigation have large permittivities and thus large a. c. conductivities as compared to semiconductors like germanium and silicon. The frequency exponent s generally increases as the permittivity, conductivity and molecular length decrease. This attenuation factor, s, is very useful in defining the general character of the sample.

The chemical structure and molecular length have been shown to affect the permittivity and conductivity in a predictable manner. The observation of hyperelectronic polarization is not dependent on molecular structure, provided the polymer is ekaconjugated. Table XVII shows the range of values for the types of polymers investigated here and the CS_2 polymer studied by Jonscher and Chan (139).

TABLE XVII

POLYMERS EXHIBITING HYPERELECTRONIC POLARIZATION

Polymer	Permittivity Range
Quinazone polymer	10 - 500
Cu-coordination polymer	30 - 100
Calcium doped pyropolymer	100 - 500
Pyropolymer	25 - 10,000
PAQR polymer	10 - 300,000
CS_2 polymer	100 - 20,000

Suggestions for Further Study

An investigation employing very high pressure of 100 kilobars or more may permit one to determine the limit of molecular orbital overlap and the related conduction and dielectric properties. An increase in the temperature range to include liquid nitrogen and liquid helium temperatures might enable one to investigate possible impurity levels existing in these samples and their influence on the permittivity and conductivity.

An apparatus which would increase the frequency range might prove useful in the determination of the behavior of hyperelectronic polarization. Higher frequencies would permit a more detailed study of the conduction hopping mechanism, while lower frequencies may reveal the relaxation times for the polarization mechanism.

Improved polymerization techniques, which could control the molecular length for a wide range, would greatly aid the quantitative investigation of hyperelectronic polarization. Of course, a soluble polymer which exhibits the properties required would be most desirable.

The investigation of hyperelectronic polarization should be extended to other amorphous semiconductors similar to CS_2. A general more rigorous theoretical calculation should be developed which could be applied to any material exhibiting hyperelectronic polarization.

BIBLIOGRAPHY

1. R. Rosen and H. A. Pohl, J. Polym. Sci. $\underline{1A}$, 1135 (1966).

2. A. R. von Hippel, Dielectrics and Waves (John Wiley and Sons, Inc., New York, 1954).

3. R. D. Hartman, unpublished Ph.D. Thesis, Oklahoma State University (1968).

4. A. Szent-Györgyi, Nature $\underline{148}$, 157 (1941).

5. A. Szent-Györgyi, Science $\underline{93}$, 609 (1941).

6. D. D. Eley, Nature $\underline{162}$, 819 (1948).

7. H. Akamatu and H. Inokuchi, J. Chem. Phys. $\underline{18}$, 810 (1950).

8. H. Inokuchi, Bull. Chem. Soc. Japan $\underline{24}$, 222 (1951).

9. H. Inokuchi, Bull. Chem. Soc. Japan $\underline{25}$, 28 (1952).

10. H. Akamatu, H. Inokuchi and Y. Matsunaga, Nature $\underline{173}$, 168 (1954).

11. H. Inokuchi, Bull. Chem. Soc. Japan $\underline{28}$, 570 (1955).

12. H. Akamutu, H. Inokuchi and Y. Matsunaga, Bull. Chem. Soc. Japan $\underline{29}$, 213 (1956).

13. D. D. Eley, H. Inokuchi and M. R. Willis, Discs. Faraday Soc. $\underline{28}$, 54 (1959).

14. Y. Harada, Y. Maruyama, I. Shirotani and H. Inokuchi, Bull. Chem. Soc. Japan $\underline{37}$, 1378 (1964).

15. H. Inokuchi and H. Akamatu, Solid State Phys. $\underline{12}$, 93 (1961).

16. I. Shirotani, H. Inokuchi and S. Minomura, Tech. Rep. of ISSP, Ser. A., No. 184 (1965).

17. I. Shirotani, H. Inokuchi and S. Minomura, Bull. Chem. Soc. Japan $\underline{39}$, 386 (1966).

18. Y. Matsunaga, Canad. J. Chem. $\underline{38}$, 323 (1960).

19. Y. Matsunaga and C. A. McDowell, Nature $\underline{185}$, 916 (1960).

20. K. Kuwatta, Y. Sato and K. Hirota, Bull. Chem. Soc. Japan 37, 1391 (1964).

21. K. Kuwatta, Y. Kageyama and K. Hirota, Bull. Chem. Soc. Japan 38, 510 (1965).

22. D. D. Eley, G. D. Parfitt, M. J. Perry and D. H. Taysun, Trans. Faraday Soc. 49, 79 (1953).

23. D. D. Eley and G. D. Parfitt, Trans. Faraday Soc. 51, 1529 (1955).

24. D. D. Eley and D. I. Spivey, Trans. Faraday Soc. 56, 1432 (1960).

25. D. D. Eley and D. I. Spivey, Trans. Faraday Soc. 58, 405 (1962).

26. D. D. Eley and D. I. Spivey, Trans. Faraday Soc. 58, 411 (1962).

27. S. Kanda and H. A. Pohl, Organic Semiconducting Polymers, Ed. J. E. Katon (Marcel Dekker, Inc., New York, 1968), p. 87.

28. H. Inokuchi, Bull. Chem. Soc. Japan 28, 570 (1955).

29. A. S. Balchan and H. G. Drickamer, Rev. Sci. Inst. 32, 305 (1961).

30. D. R. Stephens and H. G. Drickamer, J. Chem. Phys. 30, 1518 (1959).

31. S. Minomura and H. G. Drickamer, J. Phys. Chem. Solids 23, 451 (1962).

32. G. A. Samara and H. G. Drickamer, J. Phys. Chem. Solids 23, 457 (1962).

33. G. A. Samara and H. G. Drickamer, J. Chem. Phys. 37, 474 (1962).

34. R. B. Aust, G. A. Samara, and H. G. Drickamer, J. Chem. Phys. 41, 2003 (1964).

35. R. B. Aust, W. H. Bentley and H. G. Drickamer, J. Chem. Phys. 41, 1856 (1964).

36. W. H. Bentley and H. G. Drickamer, J. Chem. Phys. 42, 1573 (1965).

37. H. G. Drickamer, Solid State Phys. 17, 1 (1965).

38. H. Ohigashi, I. Shirotani, H. Inokuchi, and S. Minomura, J. Chem. Phys. 43, 314 (1965).

39. H. Inokuchi, I. Shirotani and S. Minomura, Bull. Chem. Soc. Japan 37, 1234 (1964).

40. H. Ohigashi, I. Shirotani, H. Inokuchi and S. Minomura, J. Phys. Soc. Japan 19, 1966 (1964).

41. R. S. Bradley, J. D. Grace and D. C. Monro, Trans. Faraday Soc. <u>58</u>, 776 (1962).

42. T. N. Anderson, D. W. Wood, R. C. Livingston and H. Eyring, J. Phys. Chem. <u>70</u>, 360 (1966).

43. T. N. Anderson, D. W. Wood, R. C. Livingston and H. Eyring, J. Phys. Chem. <u>44</u>, 1259 (1966).

44. M. Schwarz, H. W. Davies and B. J. Dobriansky, J. Chem. Phys. <u>40</u>, 3257 (1964).

45. J. R. Vaisnys and R. S. Kirk, Phys. Rev. <u>141</u>, 641 (1966).

46. M. Batley and L. E. Lyons, Aust. J. Chem. <u>19</u>, 345 (1966).

47. L. S. Singer and J. Kommandeur, J. Chem. Phys. <u>34</u>, 133 (1961).

48. L. S. Singer and J. Kommandeur, Bull. Am. Phys. Soc <u>4</u>, 421 (1959).

49. G. E. Blomgren and J. Kommandeur, J. Chem. Phys. <u>35</u>, 1636 (1961).

50. B. I. Kiogon'kii et al, Vysokomol. Soedin. <u>2</u>, 1494 (1960).

51. D. Bijl, H. Kainer and A. C. Rose-Innes, J. Chem. Phys. <u>30</u>, 765 (1959).

52. A. N. Holden, W. A. Yager and F. R. Merrit, J. Chem. Phys. <u>19</u>, 1319 (1951).

53. V. E. Kholmogorov and D. N. Glebovski, Opt. Spectra <u>12</u>, 728 (1968).

54. Y. Matsunaga, J. Chem. Phys. <u>30</u>, 855 (1959).

55. R. G. Kepler, J. Chem. Phys. <u>39</u>, 3528 (1963).

56. W. Slough, Trans. Faraday Soc. <u>61</u>, 408 (1965).

57. S. E. Harrison and J. M. Assour, J. Chem. Phys. <u>40</u>, 365 (1964).

58. J. W. Eastman, G. M. Androes and M. Calvin, J. Chem. Phys. <u>36</u>, 1197 (1962).

59. K. S. Cole and R. H. Cole, J. Chem. Phys. <u>9</u>, 341 (1941).

60. S. Zaromb, J. Chem. Phys. <u>24</u>, 1110 (1956).

61. B. V. Hamon, Proc. Inst. Elec. Engrs. <u>99</u>, 151 (1962).

62. K. Shindo, Rep. Prog. Polym. Phys. Jap. <u>8</u>, 341 (1965).

63. M. E. Baird, Rev. Mod. Phys. <u>40</u>, 219 (1968).

64. J. S. Dryden and R. J. Meakins, Rev. Pure Appl. Chem. 7, 15 (1957).

65. M. Davies, J. Chim. Phys. 63, 67 (1966).

66. C. P. Smyth, J. Chim. Phys. 63, 59 (1966).

67. L. S. Taylor, IEEE Trans. Ant. and Prop. AP-13, 943 (1965).

68. R. B. Hilborn, Jr., J. Appl. Phys. 36, 1553 (1965).

69. M. L. A. Robinson and H. Roetschi, J. Phys. Chem. Solids 29, 1503 (1968).

70. K. E. Johnson, Electrochim. Acta 9, 653 (1964).

71. C. M. Huggins and A. H. Sharbaugh, J. Chem. Phys. 38, 393 (1963).

72. W. A. Yager and W. O. Baker, J. Am. Chem. Soc. 64, 2164 (1942).

73. W. O. Baker and W. A. Yager, J. Am. Chem. Soc. 64, 2171 (1942).

74. L. A. Igonin, Y. V. Ovchuinokov and Y. A. Kargin, Doklady Acad. Nauk SSSR 128, 127 (1959).

75. D. W. McCall and E. W. Anderson, J. Chem. Phys. 32, 237 (1960).

76. M. Pollak, J. Chem. Phys. 43, 908 (1965).

77. C. Brot, B. Lassin, A. H. Sharbaugh, S. I. Reynolds and D. M. White, J. Chem. Phys. 43, 3603 (1965).

78. O. H. LeBlanc, Jr. J. Chem. Phys. 35, 1275 (1961).

79. J. I. Katz, S. A. Rice, S. Choi and J. Jortner, J. Chem. Phys. 39, 1683 (1963).

80. R. Silbey, J. Jortner, S. A. Rice and M. T. Vala, Jr., J. Chem. Phys. 42, 733 (1965).

81. L. Friedman, Phys. Rev. 140, A1649 (1965).

82. J. M. Andre, J. Chem. Phys. 50, 1536 (1969).

83. R. H. Partridge, J. Chem. Phys. 49, 3656 (1968).

84. J. S. Avery and R. Mason, J. Phys. Chem. 69, 784 (1965).

85. S. Choi and S. A. Rice, Phys. Rev. Lett. 8, 410 (1962).

86. S. Choi and S. A. Rice, J. Chem. Phys. 38, 366 (1963).

87. L. E. Lyons, J. Chem. Soc. 5001 (1957).

88. L. Jansen, Phys. Rev. 112, 434 (1958).

89. B. Pullman and A. Pullman, Nature 189, 725 (1961).

90. E. Memefee and Y. Pao, J. Chem. Phys. 36, 3472 (1962).

91. J. Jortner, S. A. Rice, J. L. Katz and S. Choi, J. Chem. Phys. 42, 309 (1965).

92. T. Amos and J. Musher, J. Chem. Phys. 49, 2158 (1968).

93. M. J. S. Dewar and J. A. Hashmall, J. Chem. Phys. 49, 492 (1968).

94. R. A. Keller and H. E. Rast, Jr., J. Chem. Phys. 36, 2640 (1962).

95. R. A. Marcus, J. Chem. Phys. 43, 2643 (1965).

96. W. Maslen and C. A. Coulson, J. Chem. Soc. 4041 (1957).

97. H. C. Longuet-Higgins and L. Salem, Proc. Roy. Soc. Lon. A251, 172 (1959).

98. Y. Ooshika, J. Phys. Soc. Japan 12, 1238 (1957).

99. N. S. Bayliss, J. Chem. Phys. 16, 287 (1948).

100. M. Pollak, Phys. Rev. 133, A564 (1964).

101. F. J. Morin, Phys. Rev. 93, 1195 (1954).

102. H. J. Wintle, Photochem. and Photobiol. 6, 638 (1967).

103. A. A. Berlin, M. I. Cherkashin, O. G. Selskoia and V. E. Limanov, Vysokomol. Soedin. 1, 1817 (1959).

104. L. A. Blumfield, A. A. Berlin, N. G. Matveeva, and A. E. Kalmanson, Vysokomol. Soedin. 1, 1647 (1959).

105. A. A. Berlin and N. G. Matveeva, Vysokomol. Soedin. 1, 1643 (1959).

106. A. A. Berlin et al, Vysokomol. Soedin. 1, 1361 (1959).

107. A. A. Berlin, Dokl. Acad. Nauk SSSR 136, 1127 (1961).

108. A. A. Berlin, V. I. Liogon'kii and V. P. Parini, J. Polym. Sci. 55, 675 (1961).

109. A. A. Berlin, J. Polym. Sci. 55, 621 (1961).

110. N. N. Semenov, J. Polym. Sci. 55, 563 (1961).

111. Y. M. Paushkin et al, J. Polym. Sci. 5A, 1203 (1967).

112. G. L. Slonimski et al, Vysokomol. Soedin. A9, 1706 (1967).

113. R. McNeill and D. E. Weiss, Aust. J. Chem. <u>12</u>, 643 (1959).

114. R. McNeill, R. Sindak, J. H. Wardlaw and D. E. Weiss, Aust. J. Chem. <u>16</u>, 1056 (1963).

115. R. McNeill, D. E. Weiss and D. Willis, Aust. J. Chem. <u>18</u>, 477 (1965).

116. B. A. Bolto, R. McNeill and D. E. Weiss, Aust. J. Chem. <u>16</u>, 1090 (1963).

117. L. E. Amborski, J. Polym. Sci. <u>62</u>, 331 (1962).

118. R. D. Schultz, Rep. Space Sciences Lab, North American Aviation, October 6, 1961.

119. F. H. Winslow, W. O. Baker and W. A. Yager, J. Am. Chem. Soc. <u>77</u>, 4751 (1955).

120. H. A. Pohl and J. P. Laherrere, <u>Proc. Fourth Carbon Conf.</u>, Ed. S. Mrozowski (Pergamon Press, New York, 1960), p. 259.

121. H. A. Pohl, <u>Proc. Fourth Carbon Conf.</u>, Ed. S. Mrozowski (Pergamon Press, New York, 1960), p. 241.

122. H. A. Pohl and S. L. Rosen, <u>Proc. Fifth Carbon Conf.</u>, Vol. II. (Pergamon Press, New York, 1963), p. 113.

123. H. A. Pohl, A. Rembaum and A. Henry, J. Am. Chem. Soc. <u>84</u>, 2699 (1962).

124. H. A. Pohl and R. P. Chartoff, J. Polym. Sci. <u>2A</u>, 2887 (1964).

125. H. A. Pohl and D. A. Opp, J. Phys. Chem. <u>66</u>, 2121 (1962).

126. H. A. Pohl and E. H. Engelhardt, J. Chem. Phys. <u>66</u>, 2085 (1962).

127. H. A. Pohl, <u>Semiconduction in Molecular Solids,</u> Ed. H. A. Pohl (Ivy Curtis Press, Phila., 1960), p. 9.

128. H. A. Pohl, <u>Organic Semiconductors</u>, Ed. J. J. Brophy and J. W. Buttrey (MacMillan, New York, 1962), p. 134.

129. H. A. Pohl, <u>Modern Aspects of the Vitreous State</u>, Vol. II., Ed. J. D. Mackenzie (Butterworths, London, 1962), p. 72.

130. H. A. Pohl, J. A. Bornmann and W. Itoh, <u>Organic Semiconductors</u>, Ed. J. J. Brophy and J. W. Buttrey (MacMillan, New York, 1962), p. 142.

131. H. A. Pohl, C. G. Gogos and C. Cappas, J. Polym. Sci. <u>1A</u>, 2207 (1963).

102

132. H. A. Pohl, _Electronic Aspects of Biochemistry_ (Academic Press, Inc., New York, 1964), p. 121.

133. S. Kanda and H. A. Pohl, _Organic Semiconducting Polymers_, Ed. J. E. Katon (Marcel Dekker, Inc., New York, 1968), p. 87.

134. A. Rembaum, J. Moacanin and H. A. Pohl, Progr. Dielectrics 6, 41 (1965).

135. H. A. Pohl, _Progress in Solid State Chemistry_, Vol. I., Ed. H. Reiss (Pergamon Press, New York, 1964), p. 316.

136. J. W. Mason, H. A. Pohl and R. D. Hartman, J. Polym. Sci. 17C, 187 (1967).

137. R. D. Hartman, Proc. Okla. Acad. Sci. 47, 236 (1968).

138. R. D. Hartman and H. A. Pohl, J. Polym. Sci. 6A, 1135 (1968).

139. A. K. Jonscher and W. S. Chan (private communication).

140. J. H. T. Kho and H. A. Pohl, J. Polym. Sci. 7A, 139 (1969).

141. H. A. Pohl, J. Polym. Sci. 17C, 13 (1967).

142. F. Gutmann and L. E. Lyons, _Organic Semiconductors_ (John Wiley & Sons, Inc., New York, 1967).

143. W. A. Little, Sci. Am. 212, 21 (1965).

144. W. A. Little, J. Polym. Sci. 17C, 3 (1967).

145. L. Salem, Molec. Phys. 11, 499 (1966).

146. C. G. Kuper, Phys. Rev. 150, 189 (1966).

147. K. F. G. Paulus, Molec. Phys. 10, 381 (1966).

148. V. Z. Kresin, Phys. Lett. 24, 749 (1967).

149. R. A. Ferrell, Phys. Rev. Lett. 13, 330 (1964).

150. D. A. Krueger, Phys. Rev. Lett. 19, 563 (1967).

151. R. E. DeWames, G. W. Lehman and T. Wolfram, Phys. Rev. Lett. 13, 749 (1964).

152. W. L. McCubbin, Phys. Lett. 19, 461 (1965).

153. H. Fröhlich, Phys. Lett. 26A, 169 (1968).

154. S. H. Glarum, J. Phys. Chem. Solids 24, 1577 (1963).

155. W. A. Little, Rev. Mod. Phys. 36, 264 (1964).

156. J. Ladik, G. Biczo and A. Zawadowski, Phys. Lett. 18, 257 (1965).

157. R. D. Hartman, S. Kanda and H. A. Pohl, Proc. Okla. Acad. Sci. 45, 246 (1966).

158. C. G. Koops, Phys. Rev. 83, 121 (1951).

159. L. V. Azaroff and M. J. Buerger, The Powder Method in X-Ray Crystallography (McGraw-Hill, New York, 1958).

160. H. S. Peiser, H. P. Rooksby and A. J. C. Wilson, X-Ray Diffraction by Polycrystalline Materials (John Wright and Sons, Ltd., London, 1955).

161. H. P. Klug and L. E. Alexander, X-Ray Diffraction Procedures for Polycrystalline and Amorphous Materials (John Wiley and Sons, Inc., New York, 1954).

162. M. Pollak, Phys. Rev. 138A, 1822 (1965).

163. J. R. Wyhof and H. A. Pohl (to be published).

164. Private Communication.

165. N. F. Mott, Adv. Phys. 16, 49 (1967).

166. H. Fritzsche, IBM J. Res. Develop. 13, 515 (1969).

167. M. Pollak and T. H. Geballe, Phys. Rev. 122, 1742 (1961).

168. S. Golin, Phys. Rev. 132, 178 (1963).

169. F. Argall and A. K. Jonscher, Thin Solid Films 2, 185 (1968).

170. J. R. Wyhof and H. A. Pohl, Conference on Elec. Insul. and Dielectric Phenomena, 1969 (in press).

VITA

ℒ

John Riordon Wyhof

Candidate for the Degree of

Doctor of Philosophy

Thesis: THE NATURE OF HYPERELECTRONIC POLARIZATION

Major Field: Physics

Biographical:

Personal Data: Born in New York, New York, May 19, 1943, the
son of Walter and Helen Wyhof; married Nancy Porter Wyhof,
August 21, 1965; one daughter, Karen Renée, born October
24, 1968.

Education: Graduated from Sleepy Hollow High School in Tarry-
town, New York, in 1961; received the Bachelor of Arts
degree from Middlebury College, with a major in Physics,
in June, 1965; received the Master of Science degree from
Oklahoma State University in May, 1967; completed the re-
quirements for the Doctor of Philosophy degree in May,
1970.